International Journal of Heat and Mass Transfer 253 (2025) 127418

Contents lists available at ScienceDirect

International Journal of Heat and Mass Transfer

journal homepage: www.elsevier.com/locate/hmt

# Thermal interaction of slender geothermal boreholes with strong groundwater flows

Javier Rico [a], Miguel Hermanns [b,*]

[a] Institute for Research in Technology, ICAI School of Engineering, Comillas Pontifical University, C/ Rey Francisco 4, E-28008 Madrid, Spain
[b] Departamento de Mecánica de Fluidos y Propulsión Aeroespacial, Escuela Técnica Superior de Ingeniería Aeronáutica y del Espacio, Universidad Politécnica de Madrid, Plaza Cardenal Cisneros 3, E-28040 Madrid, Spain

ARTICLE INFO

*Keywords:*
Geothermal heat exchangers
Aquifers
Thermal interaction
Matched asymptotic expansions
Moderate Peclet numbers

ABSTRACT

Geothermal boreholes benefit from the presence of aquifers, as they promote heat exchange with the ground. Adequate modeling of this interaction is essential for the optimal design of geothermal heat exchangers, ensuring both the required thermal efficiency and economic viability of the installation. The state of the art provides an appropriate theoretical framework for creeping groundwater flows, when the Peclet number of the flow remains much smaller than unity. Although this situation is common in many installations, real-world scenarios involving high-permeability soils or energy piles can result in Peclet numbers of order unity or higher. In these cases, current models fail to correctly capture the velocity field near the borehole, leading to unsatisfactory results or the need of empirical tuning parameters. The present work aims to fill this gap in the literature by employing asymptotic expansion techniques to develop a mathematically rigorous and physically consistent model that captures the effects of strong groundwater flows. Apart from demonstrating excellent accuracy compared to high-fidelity numerical simulations, the proposed model provides a critical evaluation of the strengths and limitations of the state of the art.

## 1. Introduction

In recent years, the strategic interest in reducing dependence on fossil fuels from specific markets has intensified, motivated in part by the current geopolitical scenario. This concern aligns with the growing societal awareness of climate change, which has arisen as one of the most important challenges of the current century. This context is reflected not only in governmental policies but also in the initiatives of numerous non-governmental organizations. For instance, the European Union has established ambitious goals for 2030, aiming to reduce greenhouse gas emissions by 55% compared to 1990 levels and to ensure that 32% of the final energy consumption comes from renewable sources [1].

The aforementioned energy transition must guarantee an uninterrupted and affordable energy supply while preserving current standards of human well-being. As the heating and cooling of buildings represents a significant share of global energy consumption [2], promoting high efficient heating, ventilation, and air conditioning (HVAC) systems is essential to support this transition.

Among the available technologies, low temperature geothermal energy is considered one of the most efficient and promising possibilities thanks to its weather independence and its capacity to provide a stable and continuous thermal energy supply [3]. These systems operate by exchanging heat with the surrounding ground through a heat carrying liquid that flows within coaxial or U-shaped probes installed inside vertical boreholes like the one shown in Fig. 1. Tens or even hundreds of these boreholes are connected in series or parallel to form the geothermal heat exchanger, which is connected to a water-to-water heat pump.

Correctly predicting the long-term response of the geothermal heat exchanger is essential, as the efficiency and economic viability of the whole installation depend on it. In this context, the natural approach is to numerically solve the heat transfer problem. However, capturing the long-term response requires simulating the full three-dimensional problem over the entire lifespan of the building, typically around one hundred years. Furthermore, accurately capturing the heat transfer phenomena demands an extremely fine mesh near the slender boreholes, while the computational domain must extend over a large volume to avoid distorting the underlying physics. Hence, the computational cost of faithfully simulating a real-world geothermal heat exchanger remains prohibitively high for most engineering applications [4–9].

* Corresponding author.
*E-mail addresses:* jrcabrera@comillas.edu (J. Rico), miguel.hermanns@upm.es (M. Hermanns).

https://doi.org/10.1016/j.ijheatmasstransfer.2025.127418
Received 24 April 2025; Received in revised form 10 June 2025; Accepted 14 June 2025

**Nomenclature**

| | |
|---|---|
| $\tilde{\alpha}_n, \tilde{\beta}_n$ | Laplace-transformed integration constants of the zeroth order solution to the inner region [−] |
| $A_\ell^{(n)}, B_\ell^{(n)}$ | Real Fourier series coefficients of the angular Mathieu functions of order $n$ [−] |
| $\tilde{\mathrm{A}}_{1n}$ | Laplace-transformed integration constants of the first order correction to the inner region in the limit of creeping groundwater flows [−] |
| $\alpha_b$ | Thermal diffusivity of grout [$\mathrm{m}^2/\mathrm{s}$] |
| $\alpha_g$ | Effective thermal diffusivity of ground [$\mathrm{m}^2/\mathrm{s}$] |
| $\mathrm{ce}_n, \mathrm{se}_n$ | Angular Mathieu functions of order $n$ [−] |
| $c_{n\ell}, s_{n\ell}$ | Complex Fourier series coefficients of the angular Mathieu functions of order $n$ [−] |
| $\tilde{\mathrm{C}}_\ell$ | Laplace-transformed integration constants of the zeroth order solution to the outer region [−] |
| $d_j$ | Thickness of the wall of pipe $j$ [m] |
| $\delta_{ij}$ | Kronecker's delta [−] |
| $\Delta\theta$ | Angular deviation from the downstream direction of the borehole [rad] |
| $\varepsilon_n$ | Parameter that takes the value 2 when $n = 0$ and 1 otherwise [−] |
| $\tilde{\mathrm{f}}$ | Laplace-transformed non-dimensional fictitious heat injection rate per unit borehole length [−] |
| $\gamma$ | Euler's constant [−] |
| HVAC | Heating, Ventilation, and Air Conditioning |
| $H$ | Depth of the borehole [m] |
| $h_j$ | Convective heat transfer coefficient of pipe $j$ [$\mathrm{W}/(\mathrm{m}^2\mathrm{K})$] |
| $\imath$ | Imaginary unit [−] |
| $\mathrm{I}_n, \mathrm{K}_n$ | Modified Bessel function of the first and second kind of order $n$, respectively [−] |
| $k_b$ | Thermal conductivity of grout [$\mathrm{W}/(\mathrm{m\,K})$] |
| $k_g$ | Effective thermal conductivity of ground [$\mathrm{W/m\,K}$] |
| $k_j$ | Thermal conductivity of the wall of pipe $j$ [$\mathrm{W/m\,K}$] |
| $\kappa$ | Ratio between thermal conductivity of grout and effective thermal conductivity of ground [−] |
| $\mathrm{Ke}_n$, $\mathrm{Ko}_n$ | Modified Mathieu functions of order $n$ [−] |
| Pe | Peclet number of the groundwater flow [−] |
| $\tilde{\mathrm{q}}$ | Laplace-transformed non-dimensional heat injection rate per unit borehole length [−] |
| $q_c$ | Characteristic value for the heat injection rates per unit pipe or borehole length [W/m] |
| $q_j$, $\mathrm{q}_j$, $\tilde{\mathrm{q}}_j$ | Heat injection rate per unit pipe length of pipe $j$ [W/m], its non-dimensional counterpart [−] and its non-dimensional Laplace-transformed counterpart [−] |
| $r$, $\rho$ | Radial coordinate of the polar coordinate system centered at the borehole [m] and its non-dimensional counterpart [−] |
| $r_b$ | Radius of the borehole [m] |
| $r_j$, $\rho_j$ | Radial coordinate of the polar coordinate system centered at pipe $j$ [m] and its non-dimensional counterpart [−] |
| $r_{pj}$, $\rho_{pj}$ | Radius of pipe $j$ [m] and its non-dimensional counterpart [−] |
| $R_{pj}$, $\mathrm{R}_{pj}$ | Inner thermal resistance of pipe $j$ [$(\mathrm{m\,K})/\mathrm{W}$] and its non-dimensional counterpart [−] |
| $s$ | Non-dimensional position in the complex-valued Laplace plane [−] |
| $T$, $\Theta$, $\tilde{\Theta}$ | Perturbed grout/ground temperature [K], its non-dimensional counterpart [−] and its Laplace-transformed non-dimensional counterpart [−] |
| $t$, $\tau$ | Time [s] and its non-dimensional counterpart [−] |
| $T_\infty$ | Unperturbed ground temperature [K] |
| $T_j$, $\Theta_j$, $\tilde{\Theta}_j$ | Temperature of the fluid in pipe $j$ [K], its non-dimensional counterpart [−] and its Laplace-transformed non-dimensional counterpart [−] |
| $\tilde{\Theta}_j^{(0)}$, $\tilde{\Theta}_j^{(1)}$ | Laplace-transformed zeroth order solution and first order correction to the non-dimensional fluid temperature in pipe $j$, respectively [−] |
| $\tilde{\Theta}_{\mathrm{in}}$ | Laplace-transformed solution to the inner region [−] |
| $\tilde{\Theta}_{\mathrm{in}}^{(0)}$, $\tilde{\Theta}_{\mathrm{in}}^{(1)}$ | Laplace-transformed zeroth order solution and first order correction to the inner region, respectively [−] |
| $\tilde{\Theta}_{\mathrm{out}}$ | Laplace-transformed solution to the outer region [−] |
| $\tilde{\Theta}_{\mathrm{out}}^{(0)}$, $\tilde{\Theta}_{\mathrm{out}}^{(1)}$ | Laplace-transformed zeroth order solution and first order correction to the outer region, respectively [−] |
| $t_b$ | Characteristic transversal diffusion time [s] |
| $t_c$ | Characteristic residence time of the groundwater stream in the vicinity of the borehole [s] |
| $t_H$ | Characteristic longitudinal diffusion time [s] |
| $t_q$ | Characteristic timescale of the variations in the heating and cooling needs of the building [s] |
| $t_r$ | Characteristic residence time of the heat carrying liquid in the pipes [s] |
| $\theta, \theta_j$ | Angular coordinate of the polar coordinate system centered at the borehole and at pipe $j$, respectively [rad] |
| $\tilde{\Theta}_{bm}$ | Laplace-transformed Fourier series coefficients of the grout/ground temperature at the borehole wall [−] |
| $\tilde{\Theta}_{bm}^{(0)}$, $\tilde{\Theta}_{bm}^{(1)}$ | Laplace-transformed zeroth order solution and first order correction to the Fourier series coefficients of the grout/ground temperature at the borehole wall, respectively [−] |
| $U_\infty$ | Effective seepage velocity of the groundwater flow [m/s] |

| | |
|---|---|
| $v_\rho$ | Non-dimensional radial component of the effective velocity of the groundwater flow [−] |
| $v_\theta$ | Non-dimensional azimuthal component of the effective velocity of the groundwater flow [−] |
| $V$ | Bulk velocity of the heat carrying liquid [m/s] |
| $x$, $y$ | Cartesian coordinates centered at the borehole [m] |

Consequently, simplified theoretical models have emerged to fill this gap, offering a trade-off between accuracy and reduced computational cost. Most of these models exploit the presence of large disparities in time and length scales, allowing the problem to be divided into two distinct regions [10–12]. The near-to-the-borehole region is modeled using a network of thermal resistances that represents the quasi-steady thermal response of the grout inside the boreholes and the surrounding ground [13–15]. In contrast, the far-from-the-borehole region is treated using superposition of point-source of heat. Both regions are coupled through a representative temperature, commonly referred to as the borehole wall temperature or apparent ground temperature. These models not only show excellent agreement with experimental data and high-fidelity numerical simulations, but also possess solid mathematical justification for purely conducting grounds [16,17] and in presence of creeping groundwater flows [18,19].

But strong groundwater flows do also exist in real-world scenarios involving high-permeability soils or energy piles. Accurately forecasting the thermal response of geothermal heat exchangers in such scenarios critically depends on an adequate representation of the velocity field near the borehole. Unfortunately, existing models either fail to correctly capture this velocity field or require empirical tuning parameters [20]. Therefore, a theoretical model that fills this gap is highly desirable, particularly as energy piles have gained increasing attention in recent years [21].

To develop such a model, it is insightful to also look beyond the geothermal energy literature. In fact, the thermal interaction between geothermal boreholes and groundwater flows is mathematically equivalent to two classical problems in fluid mechanics, namely, the potential flow past a circular cylinder at small Prandtl numbers and the Darcy flow past a circular cylinder in a porous medium. Although exact solutions to the unsteady problem are not yet known, many approaches have been proposed to tackle this problem by means of boundary layer techniques or employing matched asymptotic expansion techniques [22–26]. Unfortunately, none of them provide satisfactory solutions for the here-considered problem.

To address the thermal interaction of slender geothermal boreholes with strong groundwater flows, the authors propose to follow the same two-step approach used by them for the development of a model for creeping groundwater flows [18,19]. In the first step, which is the scope of the present work, the mathematical and conceptual foundations for the model are presented. For it, matched asymptotic expansion techniques are used to exploit the disparities in time and length scales of the problem, leading to a mathematically rigorous derivation of a physically sound model. The outcome of this first step also allows the critical assessment of the merits and limits of the state of the art under conditions of strong groundwater flows. In the second step, to be addressed by the authors in a follow-up work, a self-contained and computationally efficient model will be derived from the physically sound model obtained in the first step.

Consequently, the present work is organized as follows. Section 2 describes the geometrical and physical attributes of a typical geothermal borehole, along with the relevant characteristics of the ground. Furthermore, a scale analysis is conducted to identify the disparities in time and length scales, which serve to justify and motivate the simplifications performed to address the problem. In Section 3, these disparities are exploited to formulate the thermal problem in the grout filling the borehole and the ground. Section 4 describes the asymptotic structure of the problem, considering the presence of strong groundwater flows, and derives a model using matched asymptotic expansion techniques. After that, Section 5 assesses the merits and limitations of the proposed model, by comparing its outcome to detailed numerical simulations, while Section 6 focuses on the behavior of the proposed asymptotic model under creeping groundwater flow conditions. This analysis facilitates the comprehensive assessment of the state of the art performed in Section 7. Finally, Section 8 is dedicated to the conclusions of this work.

## 2. Interaction of boreholes with aquifers

A typical geothermal borehole, like the one shown in Fig. 1, is composed of one or more coaxial or U-shaped probes placed within a drilled hole in the ground, characterized by a depth $H$ and a radius $r_b$. The heat carrying liquid flows along these probes with a bulk velocity $V$ exchanging heat with the ground. Additionally, the void between probes and the ground is filled with impermeable grout, of thermal conductivity $k_b$ and thermal diffusivity $\alpha_b$, in order to promote the heat exchange and avoid the cross-contamination of aquifers. The thermal characteristics of the grout usually differ from the effective values in the ground, namely, $k_g$ and $\alpha_g$.

Given this set of parameters, three characteristic times can be constructed, namely, the characteristic residence time $t_r \sim H/V$ of the heat carrying liquid in the probes, the characteristic transversal diffusion time $t_b \sim r_b^2/\alpha_g$, and the characteristic longitudinal diffusion time $t_H \sim H^2/\alpha_g$. Based on real-world values for the involved parameters, the following sequence of characteristic times is established: $t_r \ll t_b \ll t_H$ [16].

A fourth characteristic time, $t_q$, arises from the continuously changing HVAC needs of the building. It presents a large spectrum of values, ranging from minutes up to decades, due to the HVAC needs of the building varying on an hourly, daily, weekly, monthly and yearly basis [16]. This work focuses on the most relevant scenario where the heating/cooling needs vary slowly, characterized by $t_b \ll t_q \ll t_H$ [16].

Finally, the presence of aquifers introduces a fifth characteristic time, namely, the residence time $t_c \sim r_b/U_\infty$ of the groundwater flow in the vicinity of the borehole, being $U_\infty$ the effective seepage velocity of the groundwater stream [27]. Its ratio to the characteristic transversal diffusion time $t_b$ is of the order of the Peclet number of the groundwater flow, as this non-dimensional number measures the relative importance between the convective and diffusive terms in the energy conservation equation in the ground [23]:

$$\mathrm{Pe} = \frac{r_b U_\infty}{\alpha_g} \sim \frac{t_b}{t_c}. \tag{1}$$

In scenarios involving strong groundwater flows, the Peclet number reaches values of the order of unity or higher, leading to the following sequence of characteristic times:

$$t_r \ll t_b \sim t_c \ll t_q \ll t_H. \tag{2}$$

Unfortunately, existing models assume, either implicitly or explicitly, that the Peclet number of the problem is small compared to unity, thereby limiting their applicability to scenarios involving creeping groundwater flows. To address this situation, this work derives approximate, albeit accurate, solutions to the thermal interaction of geothermal boreholes with strong groundwater flows.

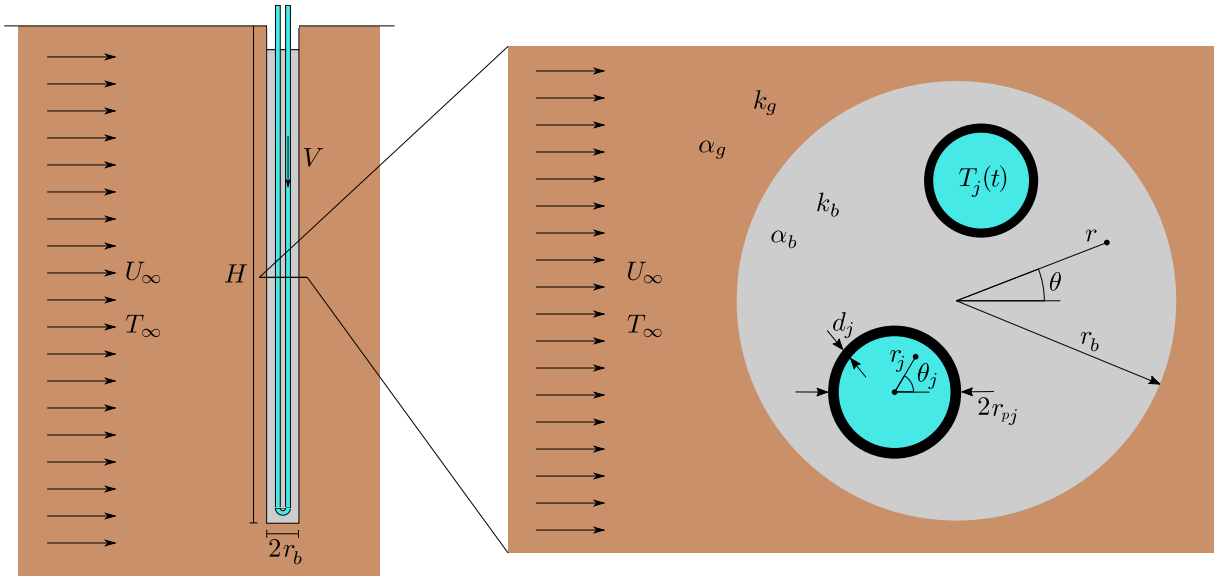


**Fig. 1.** Sketch of a vertical geothermal borehole.

## 3. Formulation of the problem

The significant disparities in time scales, particularly the fact that $t_b$ and $t_q$ are both much smaller than $t_H$, justify neglecting heat conduction along the borehole compared to radial heat conduction [16]. Additionally, since aquifers typically flow perpendicular to the boreholes due to small slopes of the piezometric pressure levels in the ground [19], the problem can be formulated in independent two-dimensional planes perpendicular to the borehole. These planes, shown in Fig. 1, are coupled to each other only through the temperatures of the heat carrying liquid.

In the ground, the porous medium approach is adopted to avoid formulating and solving the governing equations in the small voids of the soil [23]. As diffusion dominates over convection at the pore scale, Darcy's law applies for the fluid motion and thermal dispersion is considered negligible [18,23]. For the same reason, local thermal equilibrium is assumed between the groundwater and the solid matrix so that a single conservation equation is enough to describe the convective and conductive transport of heat in the ground [23].

For convenience, the problem is presented next in its non-dimensional form. To do so, the borehole radius $r_b$ is selected as characteristic length, so that $\rho$ and $\rho_j$ arise as non-dimensional radial coordinates centered at the borehole and at each pipe $j$, respectively. Similarly, the characteristic transversal diffusion time $r_b^2/\alpha_g$ is chosen as time scale, giving rise to the non-dimensional time $\tau = \alpha_g t/r_b^2$. Additionally, the characteristic heat injection rate per unit pipe length $q_c$, along with the thermal conductivity of the ground $k_g$, defines the characteristic temperature difference $q_c/k_g$. These are used to non-dimensionalize the heat injection rate per unit pipe length $q_j$ and the various temperatures of the problem:

$$\mathrm{q}_j = \frac{q_j}{q_c}, \qquad \Theta = \frac{T - T_\infty}{q_c/k_g}, \qquad \text{and} \qquad \Theta_j = \frac{T_j - T_\infty}{q_c/k_g}. \tag{3}$$

In these expressions $T$ represents the grout/ground temperature and $T_j$ the temperature of the heat carrying liquid in pipe $j$. Finally, $T_\infty$ stands for the unperturbed ground temperature far away from the borehole.

To address the unsteady nature of the problem, its formulation is done in the complex-valued Laplace plane, following the approach established in previous works [18,19]. Consequently, the energy conservation equation in the ground is expressed in terms of Laplace-transformed variables, denoted by a tilde, and the non-dimensional position $s$ in the Laplace plane. Using the polar coordinate system $(\rho, \theta)$ centered at the borehole, the equation is written as follows,

$$s\tilde{\Theta} + \mathrm{Pe}\left[\mathrm{v}_\rho \frac{\partial\tilde{\Theta}}{\partial\rho} + \frac{\mathrm{v}_\theta}{\rho}\frac{\partial\tilde{\Theta}}{\partial\theta}\right] = \frac{1}{\rho}\frac{\partial}{\partial\rho}\left(\rho\frac{\partial\tilde{\Theta}}{\partial\rho}\right) + \frac{1}{\rho^2}\frac{\partial^2\tilde{\Theta}}{\partial\theta^2}, \tag{4}$$

where the left-most term corresponds to thermal inertia of the ground and the right hand side to heat conduction in the ground. The remaining terms on the left hand side represent the convective transport of heat, with the polar components of the effective velocity field of the groundwater flow, non-dimensionalized with the effective seepage velocity $U_\infty$ of the unperturbed stream, resulting from solving the fluid-mechanical problem in the porous ground [18,19,28]:

$$\mathrm{v}_\rho = \left(1 - \frac{1}{\rho^2}\right)\cos\theta \qquad \text{and} \qquad \mathrm{v}_\theta = -\left(1 + \frac{1}{\rho^2}\right)\sin\theta. \tag{5}$$

All assumptions previously discussed for the ground also hold for the grout inside the borehole, except that no convection is acting. Consequently, the two-dimensional energy conservation equation inside the borehole is expressed, once non-dimensionalized and transformed to the complex-valued Laplace plane, as follows:

$$s\frac{\alpha_g}{\alpha_b}\tilde{\Theta} = \frac{1}{\rho}\frac{\partial}{\partial\rho}\left(\rho\frac{\partial\tilde{\Theta}}{\partial\rho}\right) + \frac{1}{\rho^2}\frac{\partial^2\tilde{\Theta}}{\partial\theta^2}, \tag{6}$$

where the ratio of the effective thermal diffusivity of the ground $\alpha_g$ and the thermal diffusivity of grout $\alpha_b$ arises.

The sought solution to the problem must also satisfy continuity conditions in temperatures and normal heat fluxes at the borehole wall. These lead to the following two conditions at $\rho = 1$:

$$\tilde{\Theta}\Big|_{\rho=1^-} = \tilde{\Theta}\Big|_{\rho=1^+} \qquad \text{and} \qquad -\kappa \frac{\partial \tilde{\Theta}}{\partial \rho}\Big|_{\rho=1^-} = -\frac{\partial \tilde{\Theta}}{\partial \rho}\Big|_{\rho=1^+}, \tag{7}$$

where $\kappa$ denotes the ratio of the thermal conductivity of grout $k_b$ and the effective thermal conductivity of the ground $k_g$.

Furthermore, a boundary condition at the outer radius $r_{pj}$ of each pipe $j$ inside the borehole must be specified as well, for which a polar coordinate system $(\rho_j, \theta_j)$ centered at each pipe $j$ is introduced for convenience [19]. The resulting condition, enforced at $\rho_j = \rho_{pj} \equiv r_{pj}/r_b$, is

$$-\rho_{pj}\kappa \frac{\partial \tilde{\Theta}}{\partial \rho_j}\Big|_{\rho_j=\rho_{pj}} = \frac{\tilde{\Theta}_j - \tilde{\Theta}\big|_{\rho_j=\rho_{pj}}}{\mathrm{R}_{pj}}. \tag{8}$$

The non-dimensional inner thermal resistance of pipe $j$, $\mathrm{R}_{pj}$, embraces all heat transfer phenomena from the heat carrying liquid at $\tilde{\Theta}_j$ up to the pipe's outer wall at $\tilde{\Theta}|_{\rho_j=\rho_{pj}}$. In this problem, two different phenomena are included [16]. First, the turbulent transport of heat inside the fluid, conveniently modeled with a convective heat transfer coefficient $h_j$ [29]. Second, the quasi-steady heat conduction occurring through the pipe's wall, of thickness $d_j$ and thermal conductivity $k_j$:

$$\mathrm{R}_{pi} = \frac{k_g}{(r_{pj} - d_j)h_j} + \frac{k_g}{k_j} \ln\left(\frac{r_{pj}}{r_{pj} - d_j}\right). \tag{9}$$

Eq. (8) alone does not fully define the mathematical problem as it involves the temperature $\tilde{\Theta}_j$ of the heat carrying liquid in pipe $j$. Its value for each pipe $j$ inside the borehole needs to be specified, either directly or indirectly, in order to complete the formulation of the problem.

In the present work, the quantity of interest to enforce onto each pipe $j$ is the heat injection rate per unit pipe length $\tilde{\mathrm{q}}_j$:

$$\tilde{\mathrm{q}}_j = \int_{-\pi}^{\pi} -\kappa \frac{\partial \tilde{\Theta}}{\partial \rho_j}\Big|_{\rho_j=\rho_{pj}} \rho_{pj} \mathrm{d}\theta_j. \tag{10}$$

To establish a relationship between the fluid temperature in pipe $j$ and the corresponding heat injection rate per unit pipe length, Eq. (8) is integrated azimuthally over pipe $j$ and combined with Eq. (10). The result is an explicit expression for the temperature $\tilde{\Theta}_j$ of the heat carrying liquid in terms of the prescribed value for $\tilde{\mathrm{q}}_j$ [18]:

$$\tilde{\Theta}_j = \frac{\mathrm{R}_{pj}}{2\pi}\tilde{\mathrm{q}}_j + \frac{1}{2\pi}\int_{-\pi}^{\pi} \tilde{\Theta}\Big|_{\rho_j=\rho_{pj}} \mathrm{d}\theta_j. \tag{11}$$

Finally, the boundary condition far from the borehole becomes homogeneous thanks to the chosen non-dimensionalization for the ground temperature:

$$\rho \to \infty : \ \tilde{\Theta} \to 0. \tag{12}$$

## 4. Asymptotic solution

The heat transfer problem to solve comprises two energy conservation equations, Eq. (4) and (6). Additionally, the problem includes continuity conditions across the borehole wall, Eq. (7), as well as boundary conditions at the pipes, Eq. (8) and (11). Finally, the condition at infinity is specified in Eq. (12).

Since obtaining an exact solution is not feasible, this work employs matched asymptotic expansion techniques to derive an approximate, albeit accurate, solution to the aforementioned problem. These techniques exploit the presence of small parameters to decompose complex problems into simpler ones [30]. Therefore, they are particularly well-suited for the present work given the presence of the small parameter $t_b/t_q \ll 1$.

### 4.1. Two-region structure

Consider the energy conservation equation in the ground, Eq. (4), and estimate the order of magnitude of each term within the equation:

$$\underbrace{s\tilde{\Theta}}_{\sim |s|} + \mathrm{Pe}\Bigg[\underbrace{\mathrm{v}_\rho \frac{\partial \tilde{\Theta}}{\partial \rho}}_{\sim \frac{\mathrm{Pe}\,\mathrm{v}_\rho}{\rho}} + \underbrace{\frac{\mathrm{v}_\theta}{\rho}\frac{\partial \tilde{\Theta}}{\partial \theta}}_{\sim \frac{\mathrm{Pe}\,\mathrm{v}_\theta}{\rho\Delta\theta}}\Bigg] = \underbrace{\frac{1}{\rho}\frac{\partial}{\partial \rho}\left(\rho \frac{\partial \tilde{\Theta}}{\partial \rho}\right)}_{\sim \frac{1}{\rho^2}} + \underbrace{\frac{1}{\rho^2}\frac{\partial^2 \tilde{\Theta}}{\partial \theta^2}}_{\sim \frac{1}{\rho^2\Delta\theta^2}}. \tag{13}$$

Regarding the left hand side of the equation, the modulus of position $s$ in the complex-valued Laplace plane governs the order of magnitude of its first term, which is related to thermal inertia of the ground. In the present work, this term is small compared to unity as $|s| \sim t_b/t_q \ll 1$ [15]. The remaining two terms of the left hand side are linked to heat convection and their orders of magnitude depend on four factors, namely, the velocity field, the Peclet number, the distance from the borehole $\rho$ and the angular deviation from the downstream direction $\Delta\theta$. Concerning the velocity field, the orders of magnitude of its components are governed by the mass conservation equation, which imposes $\mathrm{v}_\rho \sim \mathrm{v}_\theta/\Delta\theta$ [23]. Furthermore, radial component $\mathrm{v}_\rho$ is of order unity as shown in Eq. (5). Thus, both convective terms in the energy conservation equation in the ground are of order $\mathrm{Pe}/\rho$. Finally, the right-hand side of the equation represents heat conduction in the ground, which diminishes quadratically as the distance from the borehole, $\rho$, increases. This quadratic decay occurs more rapidly than the linear decay of the convective terms, allowing for the identification of two distinct regions within the problem, dependent on the distance from the borehole.

In the vicinity of the borehole, where $\rho \sim 1$, thermal inertia is negligible compared to heat convection and heat conduction due to $|s| \ll 1$ and $\mathrm{Pe} \sim 1$. Hence, this *inner region* is, in first approximation, quasi-steady and governed by conduction and convection.

Far from the borehole, particularly at distances $\rho \sim \mathrm{Pe}/|s| \gg 1$, thermal inertia and heat convection become equally relevant, while heat conduction is negligible in all directions except downstream. This is attributed to the presence of a thermal wake, where the aforementioned balance of terms slightly changes, with transversal heat conduction being also relevant in that zone [23].

The existence of this slender thermal wake has been successfully exploited in the literature on porous media and fluid mechanics to propose simplified models that solve the problem in the outer region [23]. Unfortunately, these models are based on simplifications that, albeit accurate for $\mathrm{Pe} \sim 1$, do not allow to recover valid results for small values of the Peclet number. Since authors' ultimate goal is to develop an unified model that works well for any Peclet number, this approach is not pursued in the present work. Instead, all conductive terms, both transversal and radial, are retained throughout the entire outer region, following the asymptotic framework outlined in Rico and Hermanns (2024) [18].

### 4.2. Matched asymptotic expansion techniques

The aforementioned two-region structure is exploited by means of matched asymptotic expansion techniques [30]. These mathematical methods tackle first the inner and outer problems independently and then match their solutions at an intermediate distance in which both are valid.

To derive the solutions to the inner and outer regions, $\tilde{\Theta}_{\mathrm{in}}$ and $\tilde{\Theta}_{\mathrm{out}}$ respectively, these are expressed as polynomial expansions of the small parameter of the problem. In the present work the position $s$ in the complex-valued Laplace plane, that satisfies $|s| \sim t_b/t_q \ll 1$, acts as the small parameter of the problem and the expansions to use are

$$\tilde{\Theta}_{\mathrm{in}} = \tilde{\Theta}_{\mathrm{in}}^{(0)} + s\,\tilde{\Theta}_{\mathrm{in}}^{(1)} + \mathcal{O}\left(s^2\right) \qquad \text{and} \qquad \tilde{\Theta}_{\mathrm{out}} = \tilde{\Theta}_{\mathrm{out}}^{(0)} + s\,\tilde{\Theta}_{\mathrm{out}}^{(1)} + \mathcal{O}\left(s^2\right). \tag{14}$$

Since fluid temperatures $\tilde{\Theta}_j$ are also part of the solution to the formulated heat transfer problem, they must be expressed as polynomial expansions of the small parameter as well:

$$\tilde{\Theta}_j = \tilde{\Theta}_j^{(0)} + s\,\tilde{\Theta}_j^{(1)} + \mathcal{O}\left(s^2\right). \tag{15}$$

Through the substitution of these expansions into the governing equations, continuity conditions, and boundary conditions for both the inner and outer regions, a series of mathematical problems arises. Their sequential resolution provides the various terms of the asymptotic expansion of the solution.

### 4.3. Solution to inner region

The inner region includes the borehole and the adjacent ground located at non-dimensional distances of order unity, $\rho \sim 1$. At such distances, thermal inertia is negligible and, consequently, the thermal response of the grout filling the borehole is governed solely by heat conduction:

$$0 = \frac{1}{\rho}\frac{\partial}{\partial\rho}\left(\rho\frac{\partial\tilde{\Theta}_{\mathrm{in}}^{(0)}}{\partial\rho}\right) + \frac{1}{\rho^2}\frac{\partial^2\tilde{\Theta}_{\mathrm{in}}^{(0)}}{\partial\theta^2}. \tag{16}$$

While thermal inertia remains negligible in the ground near the borehole, both heat convection and heat conduction are equally relevant, as the Peclet number is of order unity. Hence, the governing equation in the neighboring ground is

$$\mathrm{Pe}\left[\mathrm{v}_\rho\frac{\partial\tilde{\Theta}_{\mathrm{in}}^{(0)}}{\partial\rho} + \frac{\mathrm{v}_\theta}{\rho}\frac{\partial\tilde{\Theta}_{\mathrm{in}}^{(0)}}{\partial\theta}\right] = \frac{1}{\rho}\frac{\partial}{\partial\rho}\left(\rho\frac{\partial\tilde{\Theta}_{\mathrm{in}}^{(0)}}{\partial\rho}\right) + \frac{1}{\rho^2}\frac{\partial^2\tilde{\Theta}_{\mathrm{in}}^{(0)}}{\partial\theta^2}. \tag{17}$$

The previous two equations must be solved to obtain the grout/ground temperature along with the continuity conditions at the borehole wall,

$$\tilde{\Theta}_{\mathrm{in}}^{(0)}\Big|_{\rho=1^-} = \tilde{\Theta}_{\mathrm{in}}^{(0)}\Big|_{\rho=1^+} \qquad \text{and} \qquad -\kappa\frac{\partial\tilde{\Theta}_{\mathrm{in}}^{(0)}}{\partial\rho}\bigg|_{\rho=1^-} = -\frac{\partial\tilde{\Theta}_{\mathrm{in}}^{(0)}}{\partial\rho}\bigg|_{\rho=1^+}, \tag{18}$$

the specified heat injection rates per unit pipe length,

$$\tilde{\mathrm{q}}_j = \int_{-\pi}^{\pi} -\kappa\frac{\partial\tilde{\Theta}_{\mathrm{in}}^{(0)}}{\partial\rho_j}\bigg|_{\rho_j=\rho_{pj}} \rho_{pj}\,\mathrm{d}\theta_j, \tag{19}$$

and the boundary condition enforced at the outer surface of each pipe,

$$-\rho_{pj}\kappa\frac{\partial\tilde{\Theta}_{\mathrm{in}}^{(0)}}{\partial\rho_j}\bigg|_{\rho_j=\rho_{pj}} = \frac{\tilde{\Theta}_j^{(0)} - \tilde{\Theta}_{\mathrm{in}}^{(0)}\big|_{\rho_j=\rho_{pj}}}{\mathrm{R}_{pj}}, \tag{20}$$

where the zeroth order fluid temperature $\tilde{\Theta}_j^{(0)}$ is given by

$$\tilde{\Theta}_j^{(0)} = \frac{\mathrm{R}_{pj}}{2\pi}\tilde{\mathrm{q}}_j + \frac{1}{2\pi}\int_{-\pi}^{\pi}\tilde{\Theta}_{\mathrm{in}}^{(0)}\Big|_{\rho_j=\rho_{pj}}\mathrm{d}\theta_j. \tag{21}$$

The enforcement of the boundary condition at infinity is not feasible due to the presence of the outer region. Consequently, this condition is replaced by an asymptotic matching with the solution from that outer region.

An exact solution to the formulated inner problem is unknown but, fortunately, such a solution is not required for the theoretical approach pursued in this work. What is indeed essential is deriving the general behavior of the zeroth order inner solution in the ground, which is inferred from the general solution to the governing equation there, Eq. (17):

$$\tilde{\Theta}_{\mathrm{in}}^{(0)}\Big|_{\rho\geq1} = \mathrm{e}^{\frac{\mathrm{Pe}}{2}\left(\rho+\frac{1}{\rho}\right)\cos(\theta)}\cdot\sum_{n=0}^{\infty}\left[\tilde{\alpha}_n\frac{\mathrm{Ke}_n\left(\ln\rho,\frac{\mathrm{Pe}}{2}\right)}{\mathrm{Ke}_n\left(0,\frac{\mathrm{Pe}}{2}\right)}\,\mathrm{ce}_n\left(\theta,-\frac{\mathrm{Pe}^2}{4}\right) + \tilde{\beta}_n\frac{\mathrm{Ko}_n\left(\ln\rho,\frac{\mathrm{Pe}}{2}\right)}{\mathrm{Ko}_n\left(0,\frac{\mathrm{Pe}}{2}\right)}\,\mathrm{se}_n\left(\theta,-\frac{\mathrm{Pe}^2}{4}\right)\right]. \tag{22}$$

The separation of variables method allows to express the sought solution in terms of angular Mathieu functions, $\mathrm{ce}_n$ and $\mathrm{se}_n$, and modified Mathieu functions, $\mathrm{Ke}_n$ and $\mathrm{Ko}_n$, [31,32], with $\tilde{\alpha}_n$ and $\tilde{\beta}_n$ being integration constants. More details about these special functions can be found in Appendices A and B.

One significant aspect of this analytical solution is that it inherently satisfies the boundary condition at infinity, thereby eliminating the need for matching with the outer solution to obtain the zeroth order solution to the inner problem. This implies that, at this level of approximation, no information is transferred from the outer region to the inner region. However, it is anticipated that the need for matching conditions will arise in higher-order approximations.

The proposed theoretical approach requires only the general solution within the ground. Consequently, the heat equation in the grout is not addressed, leaving the integration constants $\tilde{\alpha}_n$ and $\tilde{\beta}_n$ undetermined. To facilitate the present theoretical analysis, the aforementioned integration constants are expressed in terms of more convenient unknown coefficients, which are also a part of the solution to the zeroth inner problem, namely, the coefficients $\tilde{\Theta}_{bm}$ of the Fourier series expansion of the grout/ground temperature at the borehole wall:

$$\tilde{\Theta}_{bm} = \frac{1}{2\pi}\int_{-\pi}^{\pi} \tilde{\Theta}_{\mathrm{in}}^{(0)}\Big|_{\rho=1} \mathrm{e}^{-\imath m\theta}\,\mathrm{d}\theta, \tag{23}$$

where $\imath = \sqrt{-1}$. The sought relationship is found in two steps. First, the zeroth order inner solution in ground, Eq. (22), is evaluated at the borehole wall and equated with its corresponding expression in terms of the Fourier series coefficients $\tilde{\Theta}_{bm}$:

$$\mathrm{e}^{\mathrm{Pe}\cos(\theta)}\sum_{n=0}^{\infty}\left[\tilde{\alpha}_n \mathrm{ce}_n\left(\theta,-\frac{\mathrm{Pe}^2}{4}\right)+\tilde{\beta}_n \mathrm{se}_n\left(\theta,-\frac{\mathrm{Pe}^2}{4}\right)\right] = \sum_{m=-\infty}^{\infty}\tilde{\Theta}_{bm}\mathrm{e}^{\imath m\theta}. \tag{24}$$

Thereafter, the real-valued exponential function is moved to the right hand side of the equation to exploit the orthogonality of angular Mathieu functions discussed in Appendix A:

$$\tilde{\alpha}_n = \frac{1}{\varepsilon_n\pi}\int_{-\pi}^{\pi}\mathrm{e}^{-\mathrm{Pe}\cos(\theta)}\sum_{m=-\infty}^{\infty}\tilde{\Theta}_{bm}\mathrm{e}^{\imath m\theta}\mathrm{ce}_n\left(\theta,-\frac{\mathrm{Pe}^2}{4}\right)\mathrm{d}\theta \quad \text{and} \quad \tilde{\beta}_n = \frac{1}{\varepsilon_n\pi}\int_{-\pi}^{\pi}\mathrm{e}^{-\mathrm{Pe}\cos(\theta)}\sum_{m=-\infty}^{\infty}\tilde{\Theta}_{bm}\mathrm{e}^{\imath m\theta}\mathrm{se}_n\left(\theta,-\frac{\mathrm{Pe}^2}{4}\right)\mathrm{d}\theta, \tag{25}$$

where $\varepsilon_0 = 2$ and $\varepsilon_n = 1$ for all other values of $n$.

Eq. (25) successfully relates the integration constants $\tilde{\alpha}_n$ and $\tilde{\beta}_n$ with the Fourier series coefficients $\tilde{\Theta}_{bm}$ of the grout/ground temperature at the borehole wall. However, this relationship can be further simplified by also expressing the angular Mathieu functions as Fourier series expansions:

$$\mathrm{ce}_n\left(\theta,-\frac{\mathrm{Pe}^2}{4}\right) = \sum_{\ell=-\infty}^{\infty}c_{n\ell}\mathrm{e}^{\imath\ell\theta} \quad \text{and} \quad \mathrm{se}_n\left(\theta,-\frac{\mathrm{Pe}^2}{4}\right) = \sum_{\ell=-\infty}^{\infty}s_{n\ell}\mathrm{e}^{\imath\ell\theta}, \tag{26}$$

where the coefficients $c_{n\ell}$ and $s_{n\ell}$ depend on the Peclet number as shown in Appendix A. Substitution of these expansions into Eq. (25) leads to

$$\tilde{\alpha}_n = \frac{1}{\varepsilon_n\pi}\sum_{m=-\infty}^{\infty}\tilde{\Theta}_{bm}\sum_{\ell=-\infty}^{\infty}c_{n\ell}\int_{-\pi}^{\pi}\mathrm{e}^{-\mathrm{Pe}\cos(\theta)}\mathrm{e}^{\imath m\theta}\mathrm{e}^{\imath\ell\theta}\mathrm{d}\theta \quad \text{and} \quad \tilde{\beta}_n = \frac{1}{\varepsilon_n\pi}\sum_{m=-\infty}^{\infty}\tilde{\Theta}_{bm}\sum_{\ell=-\infty}^{\infty}s_{n\ell}\int_{-\pi}^{\pi}\mathrm{e}^{-\mathrm{Pe}\cos(\theta)}\mathrm{e}^{\imath m\theta}\mathrm{e}^{\imath\ell\theta}\mathrm{d}\theta. \tag{27}$$

The simplification arises from the fact that the imaginary part of both integrands is odd, causing no effect on the values of $\tilde{\alpha}_n$ and $\tilde{\beta}_n$ when integrated over a $2\pi$ domain. Additionally, the integration of the remaining real part can be expressed using modified Bessel functions of the first kind $\mathrm{I}_n(z)$ [31], leading to

$$\tilde{\alpha}_n = \frac{2}{\varepsilon_n}\sum_{m=-\infty}^{\infty}\sum_{p=-\infty}^{\infty}\tilde{\Theta}_{bm}c_{np}\mathrm{I}_{m+p}(-\mathrm{Pe}) \quad \text{and} \quad \tilde{\beta}_n = \frac{2}{\varepsilon_n}\sum_{m=-\infty}^{\infty}\sum_{p=-\infty}^{\infty}\tilde{\Theta}_{bm}s_{np}\mathrm{I}_{m+p}(-\mathrm{Pe}). \tag{28}$$

#### 4.3.1. Heat injection rate per unit borehole length

In the field of geothermal energy, a commonly used quantity is the heat injection rate per unit borehole length $\tilde{\mathrm{q}}$ that represents the total amount of heat exchanged between borehole and ground per unit time and unit borehole length. Its value results from integrating the heat flux over the borehole wall:

$$\tilde{\mathrm{q}} = \int_{-\pi}^{\pi} -\frac{\partial\tilde{\Theta}_{\mathrm{in}}^{(0)}}{\partial\rho}\Big|_{\rho=1}\mathrm{d}\theta. \tag{29}$$

Introducing this quantity here is convenient as most models in the literature report their results in terms of it [10,11,16,18,27,33]. Therefore, it is particularly useful, when comparing results with the state of the art in Section 6, to establish a relationship between $\tilde{\mathrm{q}}$ and the integration constants $\tilde{\alpha}_n$ and $\tilde{\beta}_n$. For it, the zeroth order inner solution in the ground, Eq. (22), is differentiated, evaluated at the borehole wall, and substituted into Eq. (29) to obtain

$$\frac{\tilde{\mathrm{q}}}{2\pi} = -\sum_{n=0}^{\infty}\tilde{\alpha}_n\frac{\mathrm{Ke}_n'\left(0,\frac{\mathrm{Pe}}{2}\right)}{\mathrm{Ke}_n\left(0,\frac{\mathrm{Pe}}{2}\right)}\sum_{\ell=-\infty}^{\infty}c_{n\ell}\mathrm{I}_\ell(\mathrm{Pe}). \tag{30}$$

### 4.4. Solution to outer region

Far from the borehole, at non-dimensional distances of order $\rho \sim \mathrm{Pe}/|s| \gg 1$, thermal inertia and heat convection are equally relevant, while heat conduction becomes negligible in all directions except downstream of the borehole. Nonetheless, all three phenomena are retained throughout the entire outer region, following the asymptotic framework presented in Rico and Hermanns (2024) [18]. Thankfully, the governing equation with all three phenomena becomes solvable in the outer region since the velocity field far from the borehole is, in first approximation, an uniform stream:

$$\mathrm{v}_\rho\Big|_{\rho\gg1} = \cos\theta + \mathcal{O}\left(s^2\right) \quad \text{and} \quad \mathrm{v}_\theta\Big|_{\rho\gg1} = -\sin\theta + \mathcal{O}\left(s^2\right). \tag{31}$$

Hence, the zeroth order solution to the outer region must satisfy the boundary condition at infinity, Eq. (12), and the following partial differential equation:

$$s\tilde{\Theta}^{(0)}_{\text{out}} + \text{Pe}\left[\cos(\theta)\frac{\partial\tilde{\Theta}^{(0)}_{\text{out}}}{\partial\rho} - \frac{\sin(\theta)}{\rho}\frac{\tilde{\Theta}^{(0)}_{\text{out}}}{\partial\theta}\right] = \frac{1}{\rho}\frac{\partial}{\partial\rho}\left(\rho\frac{\partial\tilde{\Theta}^{(0)}_{\text{out}}}{\partial\rho}\right) + \frac{1}{\rho^2}\frac{\partial^2\tilde{\Theta}^{(0)}_{\text{out}}}{\partial\theta^2}. \tag{32}$$

The solution to the zeroth order outer problem is

$$\tilde{\Theta}^{(0)}_{\text{out}} = \text{e}^{\frac{\text{Pe}}{2}\rho\cos(\theta)}\sum_{\ell=-\infty}^{\infty}\tilde{\text{C}}_\ell\,\text{K}_\ell\left(\frac{\rho\text{Pe}}{2}\sqrt{1+\frac{4\,s}{\text{Pe}^2}}\right)\text{e}^{\imath\ell\theta}, \tag{33}$$

with $\text{K}_n(z)$ being the modified Bessel functions of the second kind [31]. The unspecified integration constants $\tilde{\text{C}}_\ell$ are determined by imposing the matching with the inner solution.

### 4.5. Matching of both regions

The final step to construct an asymptotic model by means of matched asymptotic expansion techniques consists in the matching of both solutions [30]. This process imposes that at an intermediate region located far from the borehole, $\rho \gg 1$, but closer to the borehole than the outer region, $\rho|s| \ll 1$, both solutions must be asymptotically equivalent. That is, their difference must be negligible:

$$\tilde{\Theta}^{(0)}_{\text{in}}\Big|_{\rho\gg1} - \tilde{\Theta}^{(0)}_{\text{out}}\Big|_{\rho|s|\ll1} \ll 1. \tag{34}$$

To enforce this condition, the inner solution in the ground, Eq. (22), is expressed as Fourier series in order to facilitate the term-by-term comparison with the outer solution, Eq. (33):

$$\tilde{\Theta}^{(0)}_{\text{in}}\Big|_{\rho\geq1} = \text{e}^{\frac{\text{Pe}}{2}\left(\rho+\frac{1}{\rho}\right)\cos(\theta)}\sum_{\ell=-\infty}^{\infty}\sum_{n=0}^{\infty}\left[\tilde{\alpha}_n\frac{\text{Ke}_n\left(\ln\rho,\frac{\text{Pe}}{2}\right)}{\text{Ke}_n\left(0,\frac{\text{Pe}}{2}\right)}c_{n\ell} + \tilde{\beta}_n\frac{\text{Ko}_n\left(\ln\rho,\frac{\text{Pe}}{2}\right)}{\text{Ko}_n\left(0,\frac{\text{Pe}}{2}\right)}s_{n\ell}\right]\text{e}^{\imath\ell\theta}. \tag{35}$$

Its behavior at the intermediate region is obtained by expanding the real-valued exponential function and the modified Mathieu functions for large values of $\rho$, following Appendix B:

$$\tilde{\Theta}^{(0)}_{\text{in}}\Big|_{\rho\gg1} = \text{e}^{\frac{\text{Pe}}{2}\rho(\cos(\theta)-1)}\sqrt{\frac{\pi}{\rho\,\text{Pe}}}\cdot\left[\sum_{\ell=-\infty}^{\infty}\sum_{n=0}^{\infty}\left(\frac{\tilde{\alpha}_n c_{n\ell}}{\text{Ke}_n\left(0,\frac{\text{Pe}}{2}\right)} + \frac{\tilde{\beta}_n s_{n\ell}}{\text{Ko}_n\left(0,\frac{\text{Pe}}{2}\right)}\right)\text{e}^{\imath\ell\theta} + \mathcal{O}\left(\frac{1}{\rho}\right)\right]. \tag{36}$$

This simplified version of the inner solution at the intermediate region has to be compared with the outer solution, Eq. (33), expanded for small values of $\rho|s|$ but large values of $\rho$:

$$\tilde{\Theta}^{(0)}_{\text{out}}\Big|_{\substack{\rho|s|\ll1\\ \rho\gg1}} = \text{e}^{\frac{\text{Pe}}{2}\rho(\cos(\theta)-1)}\sqrt{\frac{\pi}{\rho\,\text{Pe}}}\cdot\left[\sum_{\ell=-\infty}^{\infty}\tilde{\text{C}}_\ell\text{e}^{\imath\ell\theta} + \mathcal{O}\left(\frac{1}{\rho},\rho|s|\right)\right]. \tag{37}$$

Finally, a term-by-term comparison between the inner and outer solutions, both expanded at the intermediate region, reveals that the integration constants $\tilde{\text{C}}_\ell$ of the outer solution must be

$$\tilde{\text{C}}_\ell = \sum_{n=0}^{\infty}\left(\frac{\tilde{\alpha}_n c_{n\ell}}{\text{Ke}_n\left(0,\frac{\text{Pe}}{2}\right)} + \frac{\tilde{\beta}_n s_{n\ell}}{\text{Ko}_n\left(0,\frac{\text{Pe}}{2}\right)}\right). \tag{38}$$

## 5. Numerical examples

To assess the merits and limitations of the proposed model, a comparison with high-fidelity numerical simulations of the heat transfer problem formulated in Section 3 is carried out. All simulations are performed using the commercial software package COMSOL [34].

### 5.1. Borehole description

For all comparisons presented next, the borehole configuration depicted in Fig. 2 is used, which matches the one employed by the authors to validate earlier models [18,19]. It includes a borehole of diameter $2\,r_b = 152\,\text{mm}$ along with two heterogeneous pipes inside. Pipe 1 has an outer diameter of $2\,r_{p1} = 40\,\text{mm}$ and a wall thickness of $d_1 = 3.7\,\text{mm}$, while pipe 2 presents an outer diameter of $2\,r_{p2} = 50\,\text{mm}$ and a wall thickness of $d_2 = 4.6\,\text{mm}$. Both pipes are placed at 5 mm from the borehole wall and at $\pm45°$ from the rear stagnation point. Thus, the polar coordinates of their centers are $(51\,\text{mm}, +45°)$ and $(46\,\text{mm}, -45°)$, respectively.

The void between pipes and ground, of effective thermal conductivity $k_g = 3.00\,\text{W/(m K)}$ and effective thermal diffusivity $\alpha_g = 2.24\cdot10^{-7}\,\text{m}^2/\text{s}$, is filled with conventional grout of thermal conductivity $k_b = 1.50\,\text{W/(m K)}$ and thermal diffusivity $\alpha_b = 1.00\cdot10^{-7}\,\text{m}^2/\text{s}$.

The heat carrying liquid inside the pipes is pure water, characterized by a density of $999\,\text{kg/m}^3$, a specific heat capacity of $4184\,\text{J/(kg K)}$, a thermal conductivity of $0.577\,\text{W/(m K)}$, and a dynamic viscosity of $1.138\cdot10^{-3}\,\text{kg/(m s)}$. A turbulent flow regime is ensured in both pipes by enforcing a mass flow rate of $0.25\,\text{kg/s}$. The turbulent transport of heat within the liquid is modeled using convective heat transfer coefficients, $h_1$ and $h_2$, whose values are set using Gnielinski's correlations [29]. Their combination with the thermal conductivities of the pipes $k_1 = k_2 = 0.42\,\text{W/(m K)}$ leads to the following inner thermal resistances of the pipes:

$$R_{p1} = 0.535\frac{\text{m K}}{\text{W}} \qquad \text{and} \qquad R_{p2} = 0.544\frac{\text{m K}}{\text{W}}. \tag{39}$$

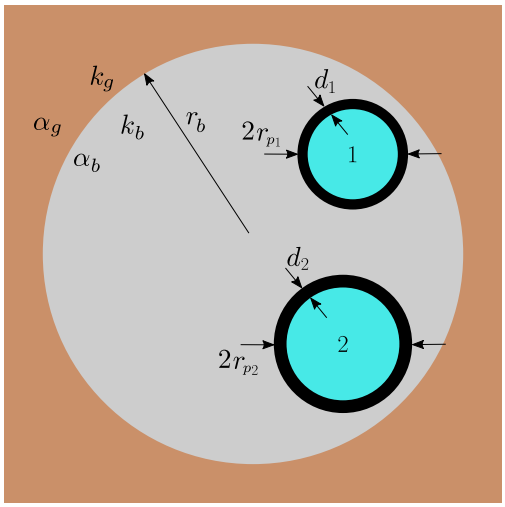


**Fig. 2.** Borehole configuration for the numerical examples.

### 5.2. Simulation procedure

The interaction between the just-described borehole and the groundwater flow involves an additional parameter, namely, the Peclet number of the groundwater flow. Two different values for the Peclet number are considered next. The first one, Pe = 1.0, demonstrates the capabilities of the here-developed asymptotic model in presence of strong groundwater flows. The second value, Pe = 0.03, assesses the performance of the present model in scenarios in which the state of the art already works well and for which the developed model is not meant for.

The following results are presented in the time domain, achieved through a two-step process. In the first step, the temperature in the Laplace domain is found by solving the reference problem formulated in Section 3 and the inner and outer problems addressed in Section 4. In the second step, the inverse Laplace transform is applied to obtain the temperature in the time domain, employing the numerical algorithm developed by the second author [35].

Finally, temporal laws governing the heat injection rates per unit pipe length are necessary as well. For the comparisons conducted in this section, time-constant values are selected, $\mathrm{q}_1(\tau) = 1$ and $\mathrm{q}_2(\tau) = 3$, whose Laplace transforms are $\tilde{\mathrm{q}}_1(s) = 1/s$ and $\tilde{\mathrm{q}}_2(s) = 3/s$, respectively.

#### 5.2.1. Reference solution

The grout/ground temperature used as benchmark is obtained from numerically solving the formulated problem presented in Section 3. This includes the governing equations for the grout and ground, Eqs. (4) and (6), along with the boundary conditions at the pipe walls, Eq. (8) and (11). Additionally, the continuity conditions at the borehole wall, Eq. (7), are enforced automatically by COMSOL.

This reference problem is formulated in an unbounded domain wherein, infinitely far from the borehole, the temperature and its Laplace-transformed counterpart are zero, Eq. (12). To ensure the accuracy of the numerical solution on a finite computational domain, a convenient domain size and shape is chosen and suitable boundary conditions are enforced at its outer rim. All details concerning the numerical solution of this problem can be found in Rico and Hermanns (2024) [18], where the same problem was addressed.

#### 5.2.2. Solution to inner region

The zeroth order solution to the inner problem is obtained by numerically solving the problem described in Section 4.3. It is comprised of the quasi-steady thermal response of grout and ground, Eq. (16) and (17), the boundary condition at the pipe walls, Eq. (20) and (21), and a zero temperature condition far from the borehole Eq. (12). Finally, the continuity conditions at the borehole wall, Eq. (18), are enforced automatically by COMSOL.

This formulation corresponds to the final steady-state of the reference problem. Therefore, the numerical characteristics chosen in the previous subsection for the reference problem, such as computational domain, mesh and boundary condition at the outer rim of the domain, are adopted as well for the numerical simulation of the inner problem.

#### 5.2.3. Solution to outer region

No numerical simulation is required to obtain the zeroth order solution to the outer region as its analytical expression, Eq. (33), is known. Nonetheless, this expression is written in terms of the integration constants $\tilde{\mathrm{C}}_\ell$, which ultimately depend on the coefficients $\tilde{\Theta}_{bm}$ of the Fourier series expansion of the zeroth order inner solution around the borehole wall. Hence, these values must be extracted from the numerical solution to the inner problem obtained with COMSOL.

To evaluate the analytical solution shown in Eq. (33), its infinite series needs to be truncated. The number of terms required to keep error levels below the desired threshold depends on the Peclet number of the groundwater flow. For small Peclet numbers, five terms are enough to achieve the accuracy level targeted in the present work. However, when the Peclet number attains values of order unity, fifteen terms are needed instead.

Additionally, integration constants $\tilde{\mathrm{C}}_\ell$ are also expressed in terms of infinite series, Eq. (38), so truncation of those series is again necessary. Fortunately, $\tilde{\alpha}_n$ and $\tilde{\beta}_n$ decrease rapidly as $n$ increases so that fifteen terms of the series are enough to accurately compute $\tilde{\mathrm{C}}_\ell$ for any Peclet number.

Finally, $\tilde{\alpha}_n$ and $\tilde{\beta}_n$ themselves are also expressed as infinite series so truncation of these series is needed again. Thankfully, Eq. (28) involves two contributions that rapidly decay in importance, the Fourier series coefficients $\tilde{\Theta}_{bm}$ and the modified Bessel functions of the first kind $\mathrm{I}_{m+p}(-\mathrm{Pe})$,

while the remaining coefficients, $c_{np}$ and $s_{np}$, are at most of order unity. Consequently, thirteen terms in $m$, ranging from $-6$ till 6, and thirty-one values of $p$, ranging from $-15$ till 15, are retained to accurately compute the values of $\tilde{\alpha}_n$ and $\tilde{\beta}_n$ for any possible Peclet number.

Once integration constants $\tilde{C}_\ell$ are obtained, Eq. (33) is implemented in Fortran 95 using the numerical algorithms developed by Donald Amos [36] for the modified Bessel functions of the second kind and by the second author [35] for the inverse Laplace transform.

### 5.3. Pe = 1.0

Temporal evolution of the grout/ground temperature for the favorable Peclet number of 1.0 is depicted in Fig. 3 through three snapshots at different times, namely, $\tau = 20$ at the top, $\tau = 50$ at the middle and $\tau = 200$ at the bottom. Inner and outer solutions are presented using solid black lines on the left and right sides of the figure, respectively, while the reference solution is plotted everywhere using a solid color map. Finally, the borehole wall and the two pipes are marked with white circles.

This figure displays the time evolution up to non-dimensional times of $\tau = 200$ as, by that time, the final steady-state is essentially reached. However, even at a tenfold lower value of $\tau = 20$, the reference solution exhibits minimal variations close to the borehole when compared to the plot corresponding to $\tau = 200$. This phenomenon is explained by the presence of the strong groundwater flow that swiftly eliminates intermediate temperature states, leading to a rapid approach to the steady-state.

As a result of this behavior, the inner solution reports excellent performance within the inner region even for the not-so-large value of $\tau = 20$. As time goes by and $\tau$ increases, the accuracy of the inner solution enhances, eventually overlapping the reference solution from $\tau = 50$ and onwards.

The outer solution exhibits great performance in all snapshots shown in Fig. 3 within its region of validity, namely, the outer region. This good performance is attributed to two reasons. First, the simplified governing equation differs from the full equation solely in the velocity field, particularly in terms that decay quadratically with $\rho$. As a result, the outer problem provides a reliable representation of the complete mathematical problem far from the borehole. Second, the coefficients of the outer solution $\tilde{C}_\ell$ are ultimately determined by the coefficients $\tilde{\Theta}_{bm}$ of the Fourier series expansion of the ground temperature around the borehole wall, via $\tilde{\alpha}_n$ and $\tilde{\beta}_n$. As demonstrated in Fig. 3, the inner region maintains high accuracy at the borehole wall, even in the unfavorable case $\tau = 20$, ensuring the precision of coefficients $\tilde{\Theta}_{bm}$. This allows the outer solution to incorporate valuable information from the inner solution through the asymptotic matching, which is reflected in the high accuracy of $\tilde{C}_\ell$.

To quantitatively assess the accuracy of the presented asymptotic model, Fig. 4 shows all three solutions along the green line depicted in the middle plot of Fig. 3 that corresponds to $\tau = 50$. This green line starts at the rear stagnation point of the borehole, at $(r, \theta) = (r_b, 0°)$, and extends downstream from the borehole.

The left side of Fig. 4 displays the temperatures from the reference solution, inner solution, and outer solution along the aforementioned green line. This plot effectively illustrates the asymptotic structure of the problem, where three distinct regions, namely, the inner region, the matching region, and the outer region, are easily identified. The right side of Fig. 4 shows the absolute errors of both inner and outer solutions along the green line, compared to the reference solution.

Close to the borehole, where the inner region is located at distances $\rho$ of order unity, the inner solution matches the reference solution with absolute/relative errors below $10^{-5}$. In contrast, the outer solution diverges significantly from the reference solution in this region, as it is outside its region of validity.

Further away from the borehole, at distances $5 < \rho < 30$, both asymptotic solutions coincide, leading to absolute (relative) errors below 0.01 (4%). This region corresponds to the intermediate distance from the borehole where the asymptotic matching between the inner and outer solutions was performed, confirming the expected agreement between both curves.

Finally, far from the borehole, where $\rho > 50$, the outer solution aligns perfectly with the reference solution, accurately predicting the temperature at locations where the borehole's thermal influence has not yet extended by $\tau = 50$. The outer solution presents absolute (relative) errors below $2 \cdot 10^{-3}$ (2%). In contrast, Fig. 4 shows how the inner solution deviates from the reference solution at these distances from the borehole, as it lies beyond its region of validity.

To complete the presentation of results, Fig. 5 displays the temporal evolution of the temperatures $\Theta_1$ and $\Theta_2$ of the heat-carrying fluid in pipes 1 and 2, respectively. These temperatures ensure that the prescribed heat injection rates per unit pipe length, $q_1(\tau) = 1$ and $q_2(\tau) = 3$, are maintained at all times. As in previous plots, the results obtained from the proposed model are compared with those from the reference solution.

The inner solution of the proposed model is time independent, leading to time-constant values for the fluid temperatures. But thermal inertia of the grout, ground, and groundwater plays an important role during the initial stages of the interaction, leading to the time-dependent evolution of the fluid temperatures seen in the reference solution. Nonetheless, the steady-state values are essentially reached by $\tau = 10$ thanks to the strong character of the groundwater flow, significantly shortening the period of time during which the inner solution is not accurate.

In practice, this inaccuracy during the initial stages of the interaction results in slightly oversized designs for the geothermal heat exchanger. If more finely tuned designs are required, the proposed model needs to be complemented by a second one specifically developed to capture the transient behavior during these initial stages. Such a two-model approach has already been successfully developed and implemented for purely conductive ground conditions [15,37,38]. In the presence of groundwater flows, though, it remains to be developed and constitutes a topic for future work.

In addition to the results reported here, further studies were carried out involving higher Peclet numbers. Although the results from these additional cases are not discussed in the present section, they align with the outcomes observed in the presented numerical example.

### 5.4. Pe = 0.03

Fig. 6 shows the time evolution of the grout/ground temperature for the unfavorable case of Pe = 0.03. Three snapshots for different times display this temporal evolution, namely, $\tau = 20$ at the top, $\tau = 200$ at the middle, and $\tau = 2000$ at the bottom. The left side of the figure shows the inner solution with solid black isolines, while the right side depicts the outer solution using the same black isolines. The reference solution is represented in both plots using a solid color map, with the borehole wall and the two pipes marked again by white circles.

Snapshots for much longer times need to be considered now. This is a consequence of the much longer times required to reach the steady-state when creeping groundwater flows are present. In fact, for $\tau = 2000$ the steady-state has still not been reached as will be discussed later. This reinforces the message that strong groundwater flows promote a fast transition to the final steady-state.

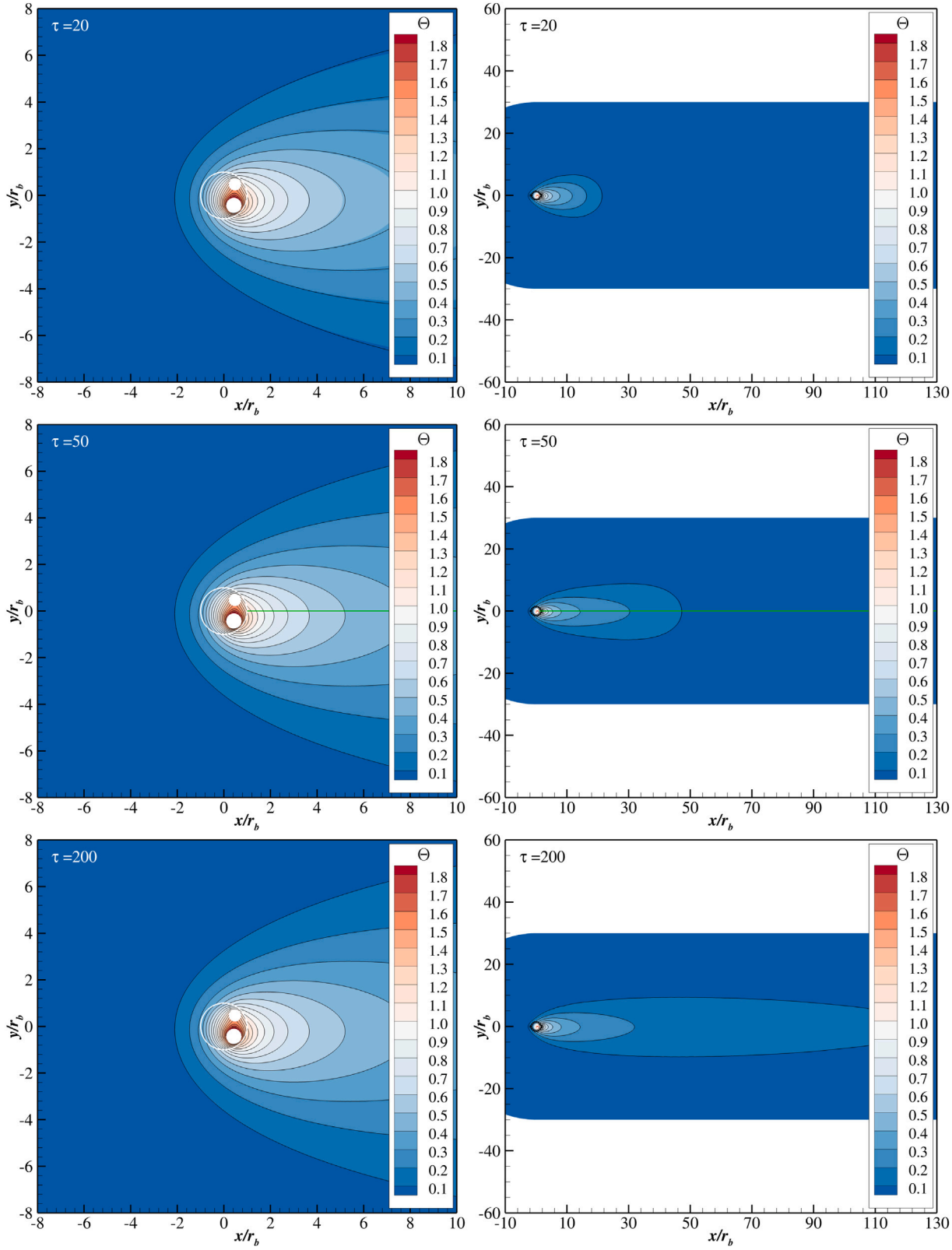


**Fig. 3.** (Left) inner solution and (right) outer solution for Pe = 1.0. Reference solution is shown as a solid color map, while inner and outer solutions are represented by black contour lines.

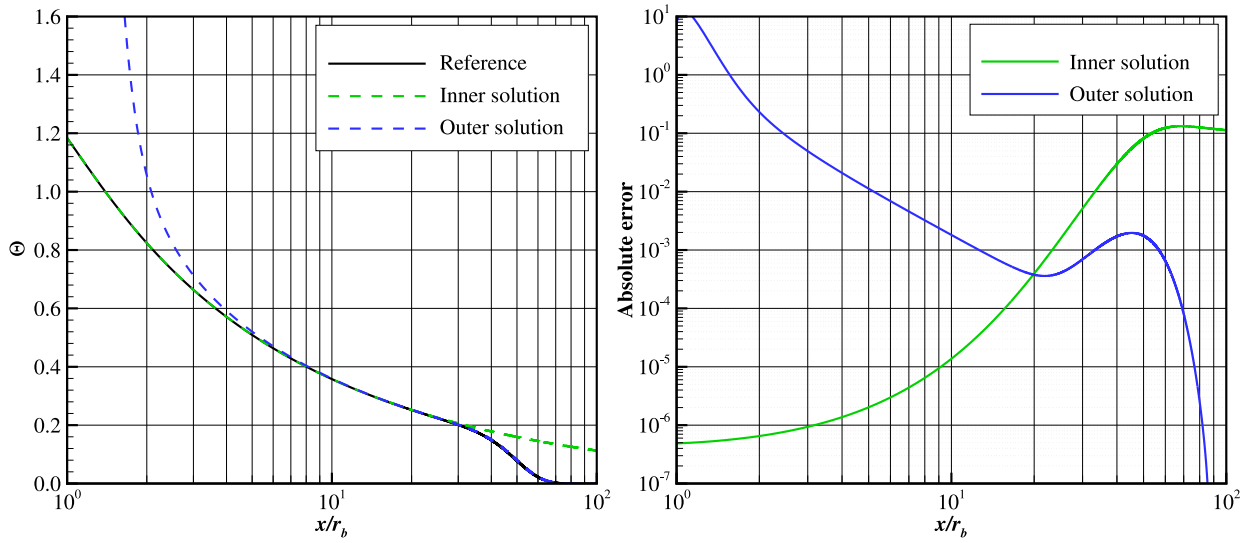


**Fig. 4.** (Left) Temperatures and (right) absolute errors along the green line represented in Fig. 3.

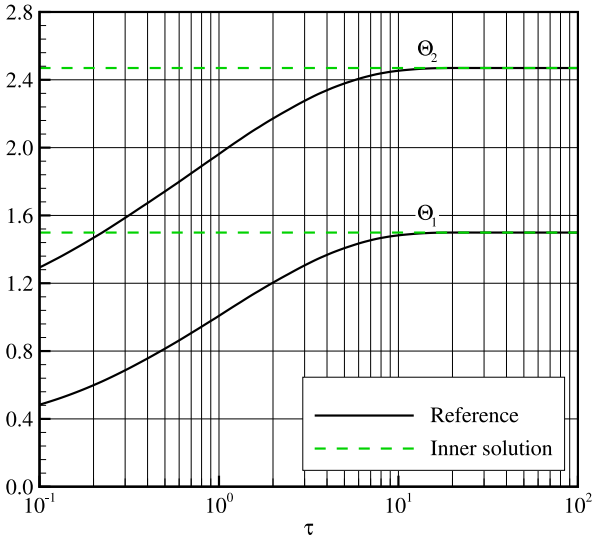


**Fig. 5.** Time evolution of the temperatures $\Theta_1$ and $\Theta_2$ of the heat carrying liquid in pipes 1 and 2, respectively, for Pe = 1.0.

Another significant difference compared to Fig. 3 is the double-fold increase in non-dimensional temperature observed in Fig. 6. This is explained by the inefficiency in transferring heat to the ground when creeping groundwater flows are present and heat conduction arises as the dominant heat transfer mechanism near the borehole.

The most unfavorable case, where Pe = 0.03 and $\tau = 20$, reveals significant discrepancies between the inner solution and the reference solution. In absence of strong groundwater flows, the inner region grows slowly, thus, for such not-so-large values of $\tau$ the quasi-steady region is narrow. This implies that the region of validity of the inner solution is very thin, failing then relatively close to the borehole. On the contrary, the outer solution demonstrates excellent performance despite the unfavorable values of Pe = 0.03 and $\tau = 20$. This exceptional result is explained similarly to the previous case: the outer solution incorporates the required information from the inner solution through asymptotic matching, and its governing equation provides a reliable representation of the full problem far from the borehole.

At later stages of the interaction, especially at $\tau = 2000$, the accuracy of the inner solution improves a lot, with its temperature isolines being almost indistinguishable from the ones of the reference solution in the close vicinity to the borehole and inside the borehole. Unfortunately, this improvement is only in part true. For creeping groundwater flows, the inner solution is decomposed into two summands [18,19]. First, a nonuniform temperature distribution that is independent of the outer solution. Second, a uniform temperature level, commonly referred to as the apparent temperature of the ground [16], that is enforced by the outer solution onto the inner solution and that simply shifts the inner solution by an additive constant without affecting its shape. Models specifically meant for creeping groundwater flows take into account this [18,19].

The present work, however, focuses on strong groundwater flows for which no information is enforced by the outer solution onto the inner solution, as explained in Section 4.3. Consequently, the proposed model is unable to recover, in the limit of creeping groundwater flows, the aforementioned apparent temperature of the ground. The proposed model, however, is able to supply the other contribution to the inner region, namely, the nonuniform temperature distribution that is independent of the outer solution. This explains the excellent overlap of the temperature isolines represented in Fig. 6, which unfortunately do not correspond to the same temperature levels.

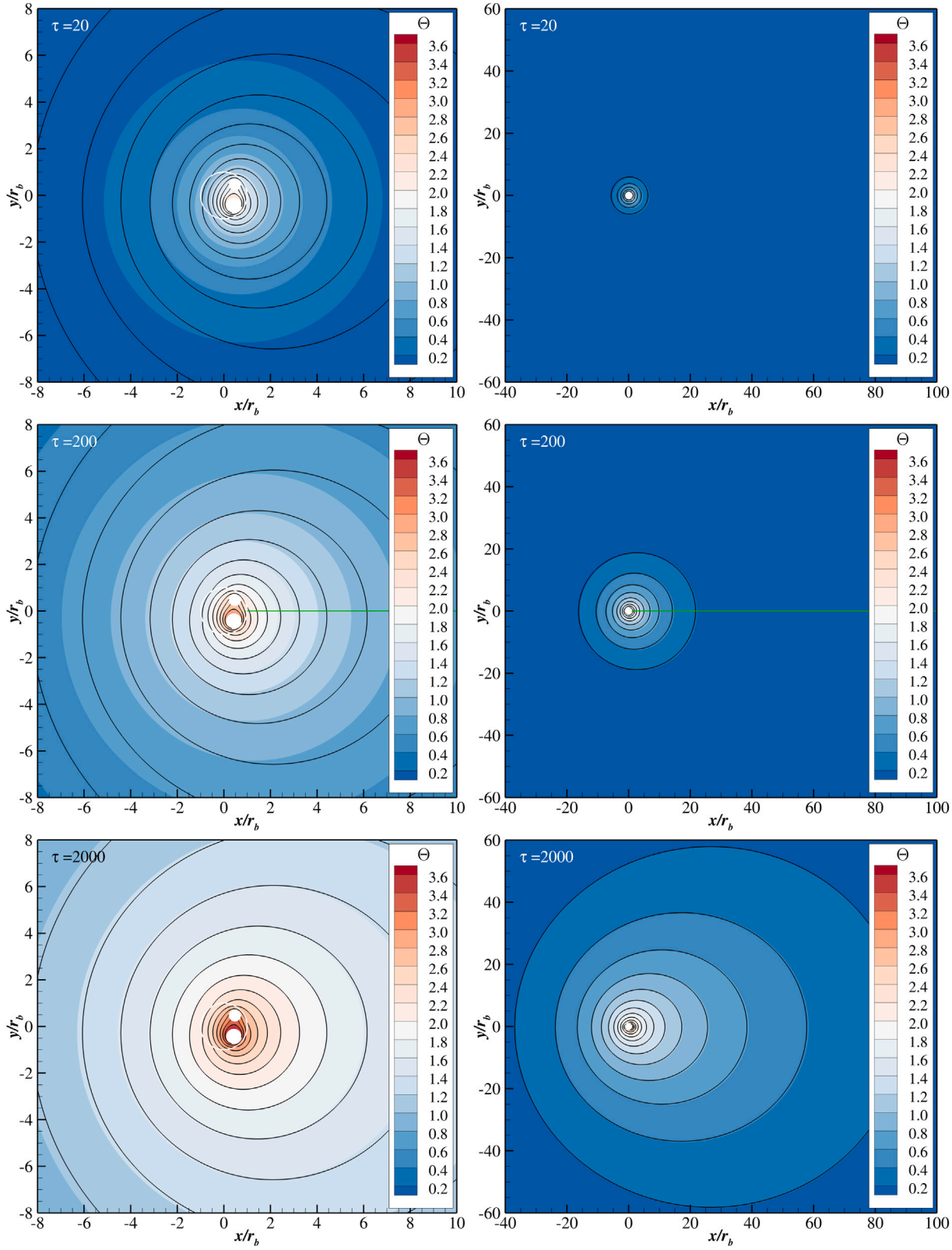


**Fig. 6.** (Left) inner solution and (right) outer solution for Pe = 0.03. Reference solution is shown as a solid color map, while inner and outer solutions are represented by black contour lines.

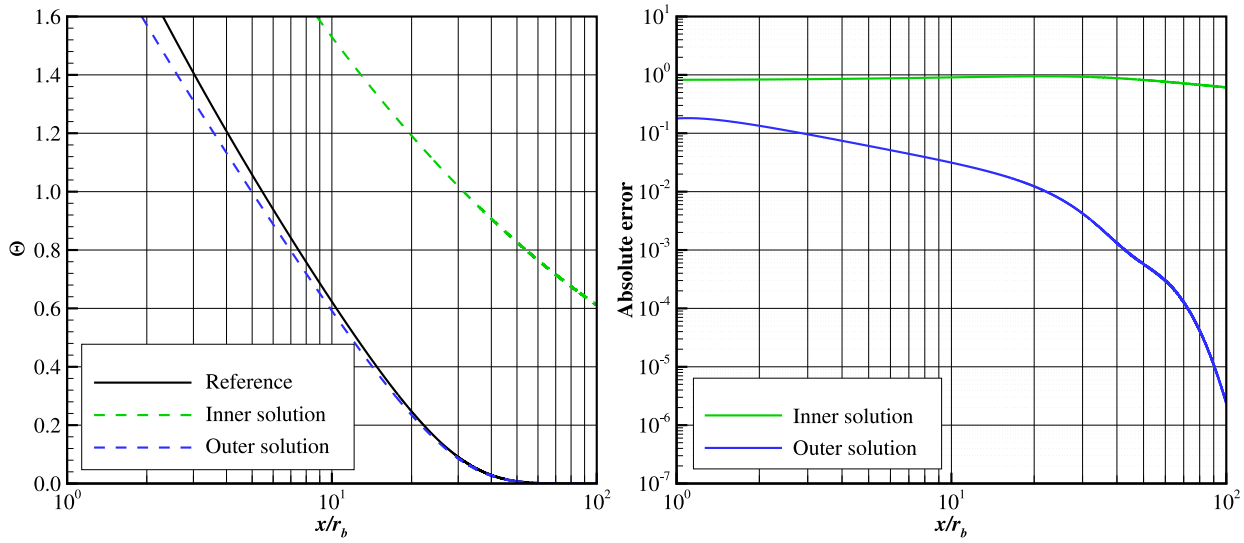


**Fig. 7.** (Left) Temperatures and (right) absolute errors along the green line represented in Fig. 6.

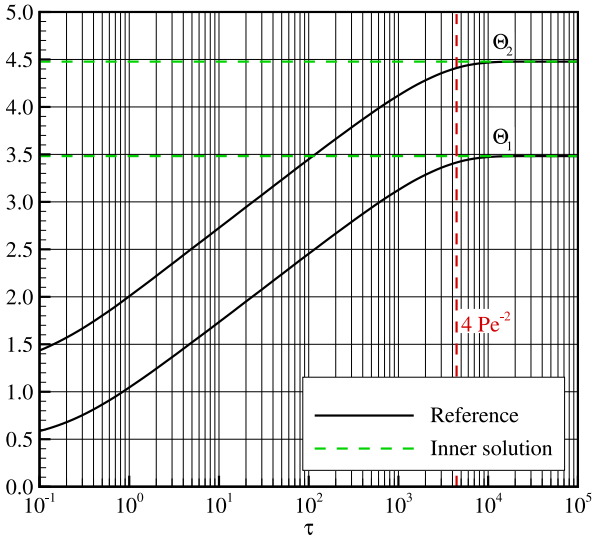


**Fig. 8.** Time evolution of the temperatures $\Theta_1$ and $\Theta_2$ of the heat carrying liquid in pipes 1 and 2, respectively, for $\mathrm{Pe} = 0.03$.

To better show this, Fig. 7 represents the inner, outer, and reference solutions evaluated along the green line shown in the middle plot of Fig. 6, corresponding to $\tau = 200$. This line, as its analogous in Fig. 3, starts at the rear stagnation point of the borehole, at $(r, \theta) = (r_b, 0°)$, and extends downstream from the borehole. The left side of Fig. 7 represents the three temperatures along this line while the right side shows the absolute errors of inner and outer solutions compared to the reference solution.

Clearly to see is that inner and reference solutions do not overlap, with absolute errors of the former one being of order unity everywhere in the inner region. Interestingly, the outer solution performs reasonably well in the inner region, well outside its region of validity. The mathematical explanation for this is given in Section 6.2.4.

To complete the presentation of results, Fig. 8 shows the continuous time evolution of the temperatures $\Theta_1$ and $\Theta_2$ of the heat carrying liquid in pipes 1 and 2, respectively. Again, the results of the proposed model are shown next to the results provided by the reference solution. As already pointed out before, the most significant change, compared to the strong groundwater case shown in Fig. 5, is the much longer time needed to reach the steady-state values for the fluid temperatures in the pipes. In fact, the required time agrees well with the estimation of $\tau \sim 4\mathrm{Pe}^{-2}$ given in the existing literature for the case of creeping groundwater flows [18,19]. Consequently, the use of models meant for strong groundwater flows to predict the response to creeping groundwater flows is not advised, and specific models for slowly moving aquifers shall be used instead.

## 6. Limit of creeping groundwater flows

The state of the art provides reliable results concerning the thermal interaction of geothermal boreholes with creeping groundwater flows [18, 27]. Hence, this section conducts an analysis of the developed asymptotic model in the limit of small Peclet numbers to facilitate a rigorous comparison with existing well-established models.

### 6.1. Inner region

An exhaustive term-by-term analysis is only accomplished for the zeroth order inner solution in the ground as no analytical expression is available for the grout. The zeroth order inner solution given by Eq. (22) is written here again to facilitate the reading of this section:

$$\tilde{\Theta}^{(0)}_{\text{in}}\Big|_{\rho\geq 1} = \mathrm{e}^{\frac{\mathrm{Pe}}{2}\left(\rho+\frac{1}{\rho}\right)\cos(\theta)} \cdot \sum_{n=0}^{\infty}\left[\tilde{\alpha}_n \frac{\mathrm{Ke}_n\left(\ln\rho, \frac{\mathrm{Pe}}{2}\right)}{\mathrm{Ke}_n\left(0, \frac{\mathrm{Pe}}{2}\right)} \mathrm{ce}_n\left(\theta, -\frac{\mathrm{Pe}^2}{4}\right) + \tilde{\beta}_n \frac{\mathrm{Ko}_n\left(\ln\rho, \frac{\mathrm{Pe}}{2}\right)}{\mathrm{Ko}_n\left(0, \frac{\mathrm{Pe}}{2}\right)} \mathrm{se}_n\left(\theta, -\frac{\mathrm{Pe}^2}{4}\right)\right]. \tag{40}$$

#### 6.1.1. Exponential function

Since distance to the borehole is of order unity in the inner region, $\rho \sim 1$, and the Peclet number is considered small compared to unity, the argument of the real-valued exponential function in Eq. (40) is small as well. Consequently, it can be approximated by the first terms of its Taylor series expansion:

$$\mathrm{e}^{\frac{\mathrm{Pe}}{2}\cos(\theta)\left(\rho+\frac{1}{\rho}\right)}\Big|_{\mathrm{Pe}\ll 1} = 1 + \frac{\mathrm{Pe}}{2}\cos(\theta)\left(\rho+\frac{1}{\rho}\right) + \mathcal{O}\left(\mathrm{Pe}^2\right). \tag{41}$$

#### 6.1.2. Mathieu functions

The zeroth order inner solution in the ground, Eq. (40), relies on the angular Mathieu functions $\mathrm{ce}_n$ and $\mathrm{se}_n$. It is well-known in the literature [31,32,39], and also shown in Appendix A, that they tend to cosine and sine functions, respectively, as their second argument, $-\mathrm{Pe}^2/4$ in this case, approaches zero:

$$\mathrm{ce}_n\left(\theta, -\frac{\mathrm{Pe}^2}{4}\right)\Big|_{\mathrm{Pe}\ll 1} = \cos(\theta) + \mathcal{O}\left(\mathrm{Pe}^2\right) \qquad \text{and} \qquad \mathrm{se}_n\left(\theta, -\frac{\mathrm{Pe}^2}{4}\right)\Big|_{\mathrm{Pe}\ll 1} = \sin(\theta) + \mathcal{O}\left(\mathrm{Pe}^2\right). \tag{42}$$

The zeroth order inner solution also depends on the modified Mathieu functions $\mathrm{Ke}_n$ and $\mathrm{Ko}_n$. Therefore, these functions must also be expanded in the limit of creeping groundwater flows. These expansions are rigorously addressed in Appendix B, as they involve some lengthy mathematical intricacies, leading to the following results for the ratios of modified Mathieu functions present in Eq. (40):

$$\begin{aligned}
&\frac{\mathrm{Ke}_0\left(\ln\rho, \frac{\mathrm{Pe}}{2}\right)}{\mathrm{Ke}_0\left(0, \frac{\mathrm{Pe}}{2}\right)}\Big|_{\mathrm{Pe}\ll 1} = 1 + \frac{\ln\rho}{\ln\left(\frac{\mathrm{Pe}}{4}\right)+\gamma} + \mathcal{O}\left(\mathrm{Pe}^2\right), \\
&\frac{\mathrm{Ke}_n\left(\ln\rho, \frac{\mathrm{Pe}}{2}\right)}{\mathrm{Ke}_n\left(0, \frac{\mathrm{Pe}}{2}\right)}\Big|_{\mathrm{Pe}\ll 1} = \frac{1}{\rho^{|n|}} + \mathcal{O}\left(\mathrm{Pe}^2\right) \qquad \forall n > 0, \\
&\frac{\mathrm{Ko}_n\left(\ln\rho, \frac{\mathrm{Pe}}{2}\right)}{\mathrm{Ko}_n\left(0, \frac{\mathrm{Pe}}{2}\right)}\Big|_{\mathrm{Pe}\ll 1} = \frac{1}{\rho^{|n|}} + \mathcal{O}\left(\mathrm{Pe}^2\right) \qquad \forall n > 0.
\end{aligned} \tag{43}$$

#### 6.1.3. Integration constants

Integration constants $\tilde{\alpha}_n$ and $\tilde{\beta}_n$ are given in terms of the coefficients $\tilde{\Theta}_{bm}$ of the Fourier series expansion of the ground temperature around the borehole wall, Eq. (28). Consequently, these coefficients need to be expanded as well as they are functions of the Peclet number of the flow:

$$\tilde{\Theta}_{bm}\Big|_{\mathrm{Pe}\ll 1} = \tilde{\Theta}^{(0)}_{bm} + \mathrm{Pe}\,\tilde{\Theta}^{(1)}_{bm} + \mathcal{O}\left(\mathrm{Pe}^2\right). \tag{44}$$

Furthermore, $\tilde{\alpha}_n$ and $\tilde{\beta}_n$ also depend on $c_{np}$ and $s_{np}$, which are the coefficients of the Fourier series expansions of the angular Mathieu functions, as well as on the modified Bessel functions of the first kind $\mathrm{I}_n$. Therefore, an analysis of their behavior as the Peclet number tends to zero is required. The former coefficients are expanded in Appendix A while the behavior of the latter functions in the limit of interest can be found in the literature [31]. By combining all aforementioned results, the expansion of the integration constants $\tilde{\alpha}_n$ and $\tilde{\beta}_n$ as the Peclet number approaches zero is obtained:

$$\begin{aligned}
&\tilde{\alpha}_0\Big|_{\mathrm{Pe}\ll 1} = \tilde{\Theta}^{(0)}_{b0} + \mathrm{Pe}\left(\tilde{\Theta}^{(1)}_{b0} - \frac{\tilde{\Theta}^{(0)}_{b(-1)} + \tilde{\Theta}^{(0)}_{b(+1)}}{4}\right) + \mathcal{O}\left(\mathrm{Pe}^2\right), \\
&\tilde{\alpha}_n\Big|_{\mathrm{Pe}\ll 1} = \tilde{\Theta}^{(0)}_{b(+n)} + \tilde{\Theta}^{(0)}_{b(-n)} - \frac{\mathrm{Pe}}{2}\left(\tilde{\Theta}^{(0)}_{b(n+1)} + \tilde{\Theta}^{(0)}_{b(n-1)} + \tilde{\Theta}^{(0)}_{b(-n+1)} + \tilde{\Theta}^{(0)}_{b(-n-1)} - 2\tilde{\Theta}^{(1)}_{b(-n)} - 2\tilde{\Theta}^{(1)}_{b(+n)}\right) + \mathcal{O}\left(\mathrm{Pe}^2\right) \qquad \forall n > 0, \\
&\tilde{\beta}_n\Big|_{\mathrm{Pe}\ll 1} = \imath\left(\tilde{\Theta}^{(0)}_{b(+n)} - \tilde{\Theta}^{(0)}_{b(-n)}\right) - \imath\frac{\mathrm{Pe}}{2}\left(\tilde{\Theta}^{(0)}_{b(n+1)} + \tilde{\Theta}^{(0)}_{b(n-1)} - \tilde{\Theta}^{(0)}_{b(-n+1)} - \tilde{\Theta}^{(0)}_{b(-n-1)} - 2\tilde{\Theta}^{(1)}_{b(-n)} - 2\tilde{\Theta}^{(1)}_{b(+n)}\right) + \mathcal{O}\left(\mathrm{Pe}^2\right) \qquad \forall n > 0.
\end{aligned} \tag{45}$$

Once each element comprising the inner solution has been analyzed separately, the outcomes are substituted into Eq. (40) to obtain the sought expansion of the inner solution in the limit of creeping groundwater flows. However, its comparison with the state of the art models is still challenging as they are commonly expressed using not only coefficients $\tilde{\Theta}^{(0)}_{bm}$ and $\tilde{\Theta}^{(1)}_{bm}$ but also the heat injection rate per unit borehole length $\tilde{\mathrm{q}}$.

To facilitate a meaningful comparison between the present model and the state of the art, an alternative expansion of the integration constant $\tilde{\alpha}_0$, that incorporates $\tilde{\mathrm{q}}$, is developed next. First, the heat injection rate per unit borehole length is written in the limit of small Peclet numbers by substituting the obtained expansions of Mathieu and Bessel functions into Eq. (30):

$$\frac{\tilde{\mathrm{q}}}{2\pi}\Big|_{\mathrm{Pe}\ll 1} = -\frac{\tilde{\alpha}_0}{\ln\left(\frac{\mathrm{Pe}}{4}\right)+\gamma} + \tilde{\alpha}_1\frac{\mathrm{Pe}}{2} + \mathcal{O}\left(\mathrm{Pe}^2\right). \tag{46}$$

This allows to express $\tilde{\alpha}_0$ in terms of the heat injection rate per unit borehole length and $\tilde{\alpha}_1$:

$$\tilde{\alpha}_0\Big|_{\mathrm{Pe}\ll 1} = \left[\ln\left(\frac{\mathrm{Pe}}{4}\right)+\gamma\right]\left(-\frac{\tilde{\mathrm{q}}}{2\pi}+\tilde{\alpha}_1\frac{\mathrm{Pe}}{2}\right)+\mathcal{O}\left(\mathrm{Pe}^2\right). \tag{47}$$

Finally, replacing $\tilde{\alpha}_1$ with its expression given in Eq. (45) leads to the sought result once all terms of order Peclet squared have been neglected:

$$\tilde{\alpha}_0\Big|_{\mathrm{Pe}\ll 1} = \left[\ln\left(\frac{\mathrm{Pe}}{4}\right)+\gamma\right]\left[-\frac{\tilde{\mathrm{q}}}{2\pi}+\frac{\mathrm{Pe}}{2}\left(\tilde{\Theta}^{(0)}_{b(+1)}+\tilde{\Theta}^{(0)}_{b(-1)}\right)\right]+\mathcal{O}\left(\mathrm{Pe}^2\right). \tag{48}$$

#### 6.1.4. Comparison with Rico and Hermanns (2024) [18]

All previous results allow to write the expansion of the inner solution for small values of the Peclet number in terms of the mean azimuthal borehole wall temperature, $\tilde{\Theta}^{(0)}_{b0}$ and $\tilde{\Theta}^{(1)}_{b0}$, and the heat injection rate per unit borehole length $\tilde{\mathrm{q}}$ in such a way that a direct comparison with the state of the art is straightforward:

$$\begin{aligned}\tilde{\Theta}^{(0)}_{\mathrm{in}}\Big|_{\mathrm{Pe}\ll 1} &= \tilde{\Theta}^{(0)}_{b0}-\frac{\tilde{\mathrm{q}}}{2\pi}\ln(\rho)+\sum_{\substack{n=-\infty\\ n\neq 0}}^{\infty}\frac{\tilde{\Theta}^{(0)}_{bn}}{\rho^{|n|}}\mathrm{e}^{\imath n\theta}\\ &+\mathrm{Pe}\left[\tilde{\Theta}^{(1)}_{b0}+\frac{\tilde{\Theta}^{(0)}_{b(+1)}+\tilde{\Theta}^{(0)}_{b(-1)}}{2}\ln(\rho)+\sum_{\substack{n=-\infty\\ n\neq 0}}^{\infty}\frac{\tilde{\mathrm{A}}_{1n}}{\rho^{|n|}}\mathrm{e}^{\imath n\theta}\right]\\ &+\mathrm{Pe}\left[\frac{\tilde{\Theta}^{(0)}_{b0}}{2}\rho\cos(\theta)-\frac{\tilde{\mathrm{q}}}{4\pi}\left(\rho+\frac{1}{\rho}\right)\ln(\rho)\cos(\theta)\right]+\mathrm{Pe}\sum_{\substack{n=-\infty\\ n\neq 0}}^{\infty}\frac{\tilde{\Theta}^{(0)}_{bn}}{4}\left[\frac{\mathrm{e}^{\imath\frac{n}{|n|}(|n|+1)\theta}}{\rho^{|n|-1}}+\frac{\mathrm{e}^{\imath\frac{n}{|n|}(|n|-1)\theta}}{\rho^{|n|+1}}\right]+\mathcal{O}\left(\mathrm{Pe}^2\right).\end{aligned} \tag{49}$$

The first row corresponds to order unity terms, while the second row introduces a correction to these terms, of the order of the Peclet number. In this correction, the coefficients $\tilde{\mathrm{A}}_{1n}$ with $n\neq 0$ are defined as follows [18]:

$$\tilde{\mathrm{A}}_{1n}=\tilde{\Theta}^{(1)}_{bn}-\frac{\tilde{\Theta}^{(0)}_{b(n+1)}+\tilde{\Theta}^{(0)}_{b(n-1)}}{4}. \tag{50}$$

The final row results from combinations of the first correction to the exponential function in Eq. (41) and the order unity terms from the first row in Eq. (49).

In comparison with the model developed by Rico and Hermanns (2024) [18], the first row is identified as the zeroth order approximation for creeping groundwater flows, while the last two rows together constitute the first order correction of the asymptotic model proposed in [18].

Although both solutions share the same structure, differences exist hidden in the expressions defining $\tilde{\Theta}^{(0)}_{b0}$ and $\tilde{\Theta}^{(1)}_{b0}$. For the present model, the corresponding expressions result from comparing Eq. (45) and (48):

$$\tilde{\Theta}^{(0)}_{b0}=-\frac{\tilde{\mathrm{q}}}{2\pi}\left[\ln\left(\frac{\mathrm{Pe}}{4}\right)+\gamma\right]\qquad\text{and}\qquad\tilde{\Theta}^{(1)}_{b0}=\frac{\tilde{\Theta}^{(0)}_{b(+1)}+\tilde{\Theta}^{(0)}_{b(-1)}}{2}\left[\ln\left(\frac{\mathrm{Pe}}{4}\right)+\gamma+\frac{1}{2}\right]. \tag{51}$$

Compared to the equivalent expressions in the creeping groundwater flow model recently proposed by the authors [18], the only difference is the absence of thermal inertia effects. This discrepancy arises because, in the latter model, the matching process between regions allows the inner region to incorporate information from the outer region, thereby including thermal inertia. In contrast, the present work neglects corrections of order $s$ as shown in Eqs. (14) and (15). Furthermore, as discussed in Section 4.3, the asymptotic matching between the two regions is not required to obtain the zeroth order approximation of the inner solution. Consequently, the inner solution developed here does not contain any information at all about thermal inertia.

As a result, the asymptotic model developed by the authors specifically for creeping groundwater flows [18] demonstrates better performance at initial times compared to the model developed in this work, as inferred from comparing Fig. 6 with Figure 5 in [18]. However, these figures also show that, as time evolves, the differences between the two models become negligible.

### 6.2. Outer solution

An exhaustive term-by-term analysis of the zeroth order outer solution is accomplished next. To enhance the readability of this section, the zeroth order outer solution obtained in Section 4.4 is shown here again:

$$\tilde{\Theta}^{(0)}_{\mathrm{out}}=\mathrm{e}^{\frac{\mathrm{Pe}}{2}\rho\cos(\theta)}\sum_{\ell=-\infty}^{\infty}\tilde{\mathrm{C}}_{\ell}\mathrm{K}_{\ell}\left(\frac{\rho\mathrm{Pe}}{2}\sqrt{1+\frac{4\,s}{\mathrm{Pe}^2}}\right)\mathrm{e}^{\imath\ell\theta}. \tag{52}$$

#### 6.2.1. Exponential function

Although in the limit of creeping groundwater flows the Peclet number is small compared to unity, $\mathrm{Pe}\ll 1$, the outer region is located at distances $\rho\mathrm{Pe}\gg 1$ [18]. Consequently, the argument of the exponential function in Eq. (52) is large and no simplification is possible.

#### 6.2.2. Integration constants

Integration constants $\tilde{\mathrm{C}}_{\ell}$ of the outer solution are dependent on three distinct sets of quantities. As shown in Eq. (38), these are the integration constants $\tilde{\alpha}_n$ and $\tilde{\beta}_n$ of the inner solution, the coefficients $c_{n\ell}$ and $s_{n\ell}$ of the Fourier series expansions of the angular Mathieu functions, and the modified Mathieu functions evaluated at the borehole wall. That is, at $\rho=1$. Consequently, the behavior of these quantities in the limit of creeping groundwater flows, which ultimately defines the behavior of $\tilde{\mathrm{C}}_{\ell}$, is discussed next.

The behavior of the integration constants of the inner solution, $\tilde{\alpha}_n$ and $\tilde{\beta}_n$, in the limit of creeping groundwater flows has already been obtained in Section 6.1.3. Hence, their resulting expansions given by Eqs. (45) and (48) are employed in the present discussion.

On the other hand, the analysis of the coefficients $c_{n\ell}$ and $s_{n\ell}$ as the Peclet number approaches zero is performed in Appendix A, where $\delta_{ij}$ stands for the Kronecker's delta:

$$c_{n\ell}\Big|_{\mathrm{Pe}\ll 1} = \frac{\epsilon_n \delta_{n|\ell|}}{2} + \mathcal{O}\left(\mathrm{Pe}^2\right) \qquad \text{and} \qquad s_{n\ell}\Big|_{\mathrm{Pe}\ll 1} = \frac{\ell}{|\ell|}\frac{\delta_{n|\ell|}}{2\imath}(1-\delta_{|\ell|0}) + \mathcal{O}\left(\mathrm{Pe}^2\right). \tag{53}$$

Finally, expansions for the modified Mathieu functions evaluated at $\rho = 1$ are also required. The mathematical derivation, with its intricate details, is reported in Appendix B leading to

$$\begin{aligned}
&\mathrm{Ke}_0\left(0, \frac{\mathrm{Pe}}{2}\right)\Big|_{\mathrm{Pe}\ll 1} = -\left[\ln\left(\frac{\mathrm{Pe}}{4}\right) + \gamma\right] + \mathcal{O}\left(\mathrm{Pe}^2\right), \\
&\mathrm{Ke}_n\left(0, \frac{\mathrm{Pe}}{2}\right)\Big|_{\mathrm{Pe}\ll 1} = \left(\frac{\mathrm{Pe}}{2}\right)^{-n} + \mathcal{O}\left(\mathrm{Pe}^{-n+2}\right) \quad \forall n > 0, \\
&\mathrm{Ko}_n\left(0, \frac{\mathrm{Pe}}{2}\right)\Big|_{\mathrm{Pe}\ll 1} = \left(\frac{\mathrm{Pe}}{2}\right)^{-n} + \mathcal{O}\left(\mathrm{Pe}^{-n+2}\right) \quad \forall n > 0.
\end{aligned} \tag{54}$$

All discussed expansions are substituted into Eq. (38) to obtain the behavior of the integration constants $\tilde{\mathrm{C}}_\ell$ in the limit of creeping groundwater flows:

$$\begin{aligned}
&\tilde{\mathrm{C}}_0\Big|_{\mathrm{Pe}\ll 1} = \frac{\tilde{\mathrm{q}}}{2\pi} - \frac{\mathrm{Pe}}{2}\left(\tilde{\Theta}^{(0)}_{b(+1)} + \tilde{\Theta}^{(0)}_{b(-1)}\right) + \mathcal{O}\left(\mathrm{Pe}^2\right), \\
&\tilde{\mathrm{C}}_{\pm 1}\Big|_{\mathrm{Pe}\ll 1} = \mathrm{Pe}\frac{\tilde{\Theta}^{(0)}_{b(\pm 1)}}{2} + \mathcal{O}\left(\mathrm{Pe}^2\right), \\
&\tilde{\mathrm{C}}_{\pm n}\Big|_{\mathrm{Pe}\ll 1} = \mathcal{O}\left(\mathrm{Pe}^{n+1}\right) \qquad \forall |n| > 1.
\end{aligned} \tag{55}$$

### 6.2.3. Comparison with Rico and Hermanns (2024) [18]

Substitution of Eq. (55) into Eq. (52) provides the following expansion for the zeroth order outer solution in the limit of creeping groundwater flows in which only terms up to order Peclet are retained:

$$\begin{aligned}
\tilde{\Theta}^{(0)}_{\mathrm{out}}\Big|_{\mathrm{Pe}\ll 1} = \; & \frac{\tilde{\mathrm{f}}}{2\pi}\mathrm{e}^{\frac{\mathrm{Pe}}{2}\rho\cos(\theta)}\mathrm{K}_0\left(\frac{\rho\mathrm{Pe}}{2}\sqrt{1+\frac{4s}{\mathrm{Pe}^2}}\right) + \mathrm{Pe}\frac{\tilde{\Theta}^{(0)}_{b(+1)}}{2}\mathrm{e}^{\frac{\mathrm{Pe}}{2}\rho\cos(\theta)}\mathrm{K}_1\left(\frac{\rho\mathrm{Pe}}{2}\sqrt{1+\frac{4s}{\mathrm{Pe}^2}}\right)\mathrm{e}^{+\imath\theta} \\
& + \mathrm{Pe}\frac{\tilde{\Theta}^{(0)}_{b(-1)}}{2}\mathrm{e}^{\frac{\mathrm{Pe}}{2}\rho\cos(\theta)}\mathrm{K}_1\left(\frac{\rho\mathrm{Pe}}{2}\sqrt{1+\frac{4s}{\mathrm{Pe}^2}}\right)\mathrm{e}^{-\imath\theta} + \mathcal{O}\left(\mathrm{Pe}^2\right),
\end{aligned} \tag{56}$$

The quantity $\tilde{\mathrm{f}}$ is the non-dimensional fictitious heat injection rate per unit borehole length first introduced in Rico and Hermanns (2024) [18]. It subtracts from the true value $\tilde{\mathrm{q}}$ the contributions of the azimuthal corrections:

$$\tilde{\mathrm{f}}(s) = \tilde{\mathrm{q}}(s) - \mathrm{Pe}\,\pi\left(\tilde{\Theta}^{(0)}_{b(+1)} + \tilde{\Theta}^{(0)}_{b(-1)}\right). \tag{57}$$

In contrast to the analysis of the inner solution presented in Section 6.1, the outer solution developed in this work includes the position $s$ in the complex-valued Laplace plane. Specifically, $s$ appears within the argument of the modified Bessel functions of the second kind $\mathrm{K}_n$, perfectly matching the literature [18,40,41]. This is expected, as the presence of the modified Bessel functions in the outer solution is due to the governing equation being solved and not from the matching process with the inner solution.

The asymptotic matching performed in this work is qualitatively different from the one developed in models for creeping groundwater flows [18,19]. The main difference, as discussed in Section 6.1.4, is the fact that the matching coefficients of the inner solution do not contain any information about thermal inertia. Consequently, no information about thermal inertia is transferred from the inner region to the outer region, leading to the absence of temporal dependence in the matching coefficients $\tilde{\mathrm{C}}_{\pm 1}$ given in Eq. (56), in contrast with the corresponding coefficients shown in Rico and Hermanns (2024) [18].

This explains the differences between Eq. (56) and Eq. (28) from Rico and Hermanns (2024) [18]. Fortunately, the absence of temporal dependence in the coefficients of the outer region is less critical compared to the inner solution, as it only affects the first order correction coefficients $\tilde{\mathrm{C}}_{\pm 1}$. Thus, results in the outer region depicted in Fig. 6 remain accurate even for short times, similar to the results shown in Figure 5 from Rico and Hermanns (2024) [18].

### 6.2.4. Analysis close to the borehole

Analogously to Rico and Hermanns (2024) [18], this subsection analyzes the behavior of the outer solution close to the borehole. Figs. 9 and 10 present two snapshots of the ground temperature close to the borehole at different times, for unfavorable $\mathrm{Pe} = 0.03$ and favorable $\mathrm{Pe} = 1.0$ cases, respectively. In these figures, the outer solution is represented using solid black lines, while the reference solution is plotted using a solid color map. Finally, the borehole wall and the two pipes are represented by white circles.

Fig. 9 shows, as expected, bad performance close to the borehole, as this region lies outside the range of validity of the outer solution. In contrast, Fig. 10 demonstrates good results even close to the borehole despite $\mathrm{Pe} = 0.03$ being outside the range of Peclet numbers considered for the model. This discrepancy in behaviors arises from the simplifications made in the velocity field to derive the outer solution. Specifically, to obtain this outer solution, the terms that deviate the velocity field from the uniform stream are neglected. However, these terms could be relevant close to the borehole since their orders of magnitude are comparable to the Peclet number. As a result, in presence of strong groundwater flows, where the Peclet number attains values of order unity, neglecting these terms leads to the bad results observed in Fig. 9. On the contrary, when creeping groundwater flows are present, the aforementioned terms are negligible everywhere in the ground, so the outer solution performs well even close to the borehole, as shown in Fig. 10.

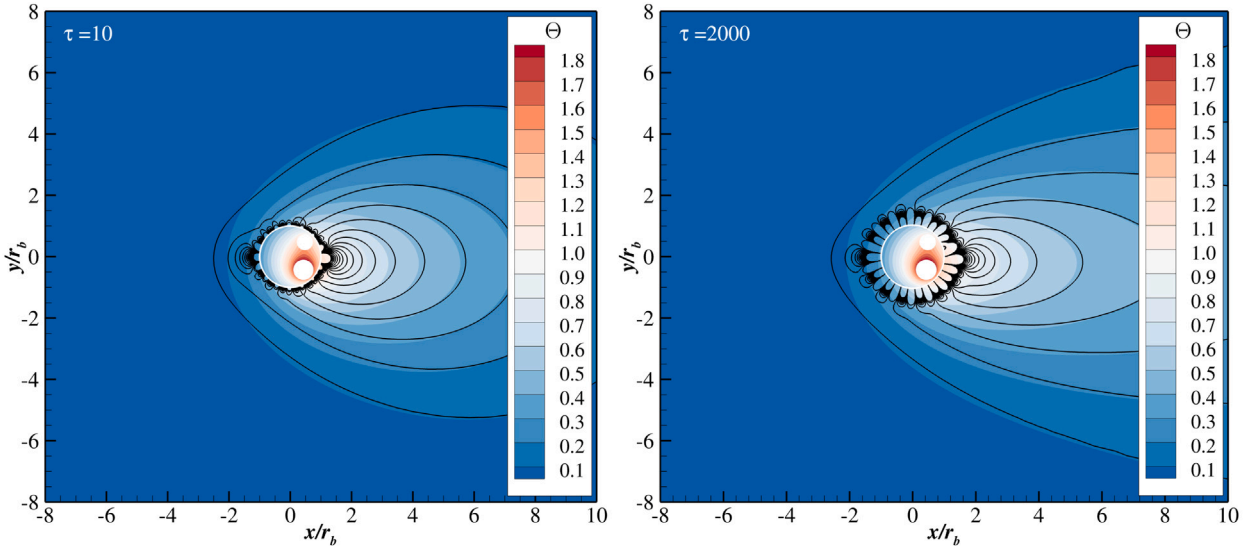


**Fig. 9.** Outer solution close to the borehole for Pe = 1.0 and (left) $\tau = 10$ and (right) $\tau = 2000$. Reference solution is shown as a solid color map, while outer solution is represented by black contour lines.

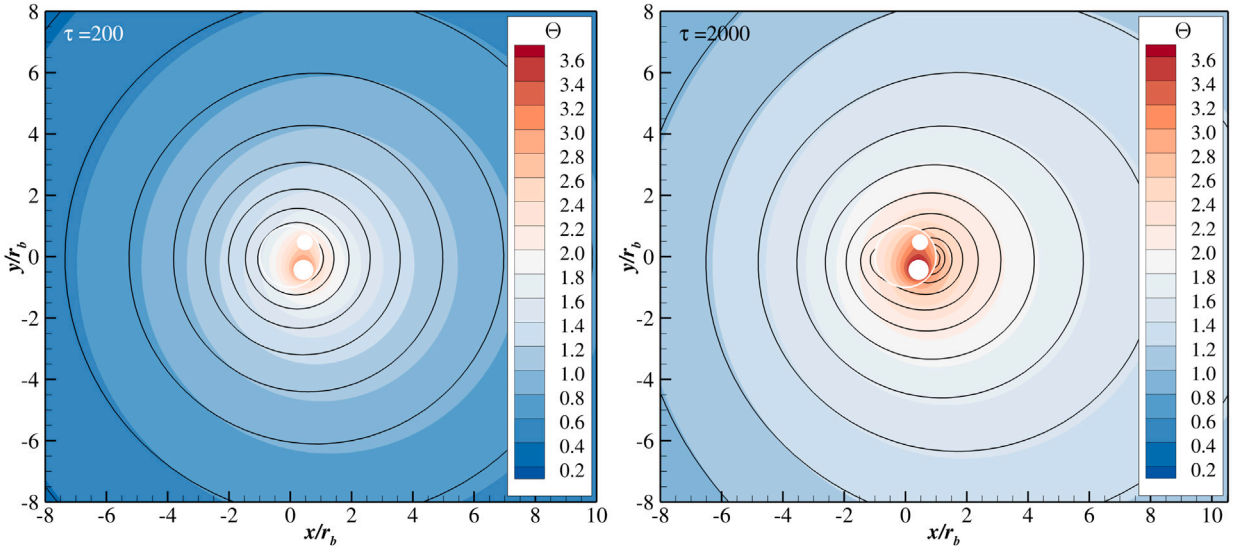


**Fig. 10.** Outer solution close to the borehole for Pe = 0.03 and (left) $\tau = 200$ and (right) $\tau = 2000$. Reference solution is shown as a solid color map, while outer solution is represented by black contour lines.

## 7. Existing models for the problem

The interaction of geothermal boreholes with groundwater flows has extensively been studied in the literature. Existing models for that interaction assume, either explicitly or implicitly, that the characteristic heat injection time $t_q$ is large compared to the characteristic transversal diffusion time $t_b$ so that the same two-region structure as in the present work emerges [18,42].

Most work in the literature is focused on the outer region to obtain there the perturbed ground temperature in terms of the heat injection rate per unit borehole length. For it, a superposition of moving point sources of heat, all of equal intensity, is used to represent the borehole. If the finite length of the borehole is thereby taken into account, so-called *moving finite line source models* result [10,43–47]. If its finite length is neglected instead, then so-called *moving infinite line source models* are obtained [27,46,48,49].

While the outer region is properly addressed by these models in the literature, as it aligns with the outer solutions presented by Rico and Hermanns (2024) [18] and in the present work, all these approaches make conceptual errors in their treatment of the inner region and its connection with the outer region.

First of all, these models typically employ a purely conductive network of thermal resistances [10,11] to represent the thermal response of the grout filling the boreholes and the surrounding ground, which constitute the inner region. This approach assumes that heat convection is negligible compared to heat conduction near the borehole, which is only correct in the presence of creeping groundwater flows where the Peclet number is small compared to unity [19].

Furthermore, once the inner region is modeled, it is linked to the outer solution through the mean azimuthal borehole wall temperature [10,11], which provides an assessment of the thermal state of the ground far from the borehole. This temperature is obtained by averaging the outer solution evaluated at the borehole wall.

This procedure contains two conceptual inconsistencies. First, in the presence of creeping groundwater flows, the temperatures that adequately represent the thermal state of the ground far from the borehole are the apparent ground temperatures at the pipes, as proven by Rico and Hermanns (2024) [19]. Although in the same work they demonstrated that, in first approximation, these apparent ground temperatures at the pipes approach the value of the mean azimuthal borehole wall temperature when the Peclet number is small compared to unity, the latter one is expected to diverge from the former ones in presence of strong groundwater flows [19]. Second, models in the literature extend the validity of the outer solution up to the borehole wall to compute the mean azimuthal borehole wall temperature. But Section 6.2.4 has shown that doing it in the presence of strong groundwater flows leads to significant errors. Consequently, the outer solution cannot be reliably used to compute the mean azimuthal borehole wall temperature for Peclet numbers of order unity.

A different approach is followed by the models recently proposed by Al-Khoury and coworkers [40,41]. They solve the heat convection–conduction problem in the ground up to the borehole wall, effectively addressing the outer and inner regions simultaneously. To obtain a solution, though, they simplify the velocity field in a way that clashes with the very existence of the borehole as they consider it uniform everywhere in the ground. Also the heat exchange inside the borehole is completely skipped by them as a uniform temperature is enforced instead at the borehole wall.

Despite these simplifications, the authors claim excellent performance of their model compared to a numerical solution. However, the numerical solution used as benchmark incorporates the same simplifications as their analytical model. Consequently, this reference solution does not properly represent the geothermal problem to solve but the simplified mathematical problem solved by Al-Khoury and coworkers using the separation of variables method.

Recently, Prieto and Cimmino (2022) [20] identified these physical inconsistencies and attempted to solve the problem in grout and ground with the correct velocity field. However, in deriving the solution for the energy conservation equation in the ground, they introduced a simplification that effectively reduced the velocity field to an uniform stream again. To overcome the resulting inaccuracy in the velocity field, they introduced a tuning parameter into their model that leads to good results for the mean azimuthal borehole wall temperature for Peclet numbers up to unity. However, the dependency of a tuning parameter along with the use of a uniform velocity field does not represent a satisfactory solution.

The interaction of geothermal boreholes with groundwater flows is mathematically equivalent to two other problems extensively studied in the field of fluid mechanics, namely, the high Reynolds-number flow past a cylinder at small Prandtl numbers and the Darcy flow past a cylinder in a porous media. In both cases the energy conservation equation to solve and the velocity field to consider are the same, playing the effective driving pressure in the latter one the role of the velocity potential in the former one.

Most work in the literature considers an uniform temperature at the cylinder wall and steady-state conditions, for which even the exact analytical solution can be found in the literature [50,51]. This involves angular and modified Mathieu functions just as the zeroth order solution to the inner region does. In fact, they are fully equivalent as both are steady-state solutions to the convection–conduction problem around a cylinder/borehole.

Although the exact analytical solution for the unsteady problem is not yet known, many approaches can be used to tackle this problem, for instance, boundary layer techniques or matched asymptotic expansion techniques [22–26]. Unfortunately, these approximate solutions are valid for small and large Peclet numbers, but not for the Peclet numbers of order unity that are of interest for the present work.

Finally, the wake approach is also used by some authors to study the thermal wake that forms behind the cylinder [22]. This wake is of relevance for the thermal interaction of neighboring boreholes as it negatively affects the performance of geothermal HVAC systems. Unluckily, the presented solutions for the thermal wake are not suited for all the Peclet numbers, so that the approach followed in the present work for the outer region, valid for all Peclet numbers, is preferred.

## 8. Conclusions

Aquifers significantly enhance the heat transfer capabilities of the ground, allowing for the construction of more compact and affordable geothermal heat exchangers. To fully exploit this improvement, theoretical models for designing and sizing geothermal heat exchangers must account for the presence of groundwater flows.

Many models exist in the literature that perform well in presence of creeping groundwater flows, i.e., when heat convection near the borehole is negligible compared to heat conduction. Among these, a previous work proposed by the authors presented a mathematically rigorous derivation of a physically sound model based on matched asymptotic expansion techniques. Two distinct asymptotic regions were identified then, namely, the inner and the outer region. While in the outer region all heat transfer mechanisms were retained, in the inner region heat convection near the borehole was neglected close to the borehole due to the creeping character of the considered groundwater flows.

However, in many real-world scenarios involving high-permeability grounds and energy piles, heat convection near the borehole is as significant as heat conduction so that existing models fail to correctly capture the velocity field in the vicinity of the borehole.

The present work seeks to address this issue and derives an analytical model that correctly retains the convective phenomenon in both asymptotic regions. In particular, a closed-form expression is derived for the outer region, while a semi-analytical solution is developed for the inner region. Comparisons with detailed numerical simulations show excellent performance of both inner and outer solutions within their ranges of validity, keeping absolute (relative) errors below 0.01 (4%). Although the model still performs well for the less favorable case of creeping groundwater flows, it does not behave as good as models specifically designed for slowly moving aquifers.

Furthermore, the proposed model has also served to assess the theoretical and conceptual merits and limits of the state of the art, clarifying why most models in the literature cannot be used in presence of strong groundwater flows.

Finally, the present work promotes further research toward the rigorous development of a purely-theoretical model for the inner region in presence of strong groundwater flows.

## CRediT authorship contribution statement

**Javier Rico:** Writing – review & editing, Writing – original draft, Visualization, Validation, Software, Formal analysis. **Miguel Hermanns:** Writing – review & editing, Writing – original draft, Supervision, Methodology, Funding acquisition, Formal analysis, Conceptualization.

## Declaration of competing interest

The authors declare that they have no known competing financial interests or personal relationships that could have appeared to influence the work reported in this paper.

## Acknowledgments

Grant PID2021-128172OB-I00 funded by MCIN/AEI/10.13039/501100011033 and by "ERDF A way of making Europe".

## Appendix A. Angular mathieu functions

In the literature, the preferred form of expressing the angular Mathieu functions $\mathrm{ce}_n$ and $\mathrm{se}_n$ is as real Fourier series expansions [31,32]:

$$\begin{aligned}
\mathrm{ce}_{2n}\left(\theta,-\frac{\mathrm{Pe}^2}{4}\right) &= (-1)^n \sum_{\ell=0}^{\infty}(-1)^{\ell} A_{2\ell}^{(2n)} \cos(2\ell\theta),\\
\mathrm{ce}_{2n+1}\left(\theta,-\frac{\mathrm{Pe}^2}{4}\right) &= (-1)^n \sum_{\ell=0}^{\infty}(-1)^{\ell} B_{2\ell+1}^{(2n+1)} \cos[(2\ell+1)\theta],\\
\mathrm{se}_{2n+1}\left(\theta,-\frac{\mathrm{Pe}^2}{4}\right) &= (-1)^n \sum_{\ell=0}^{\infty}(-1)^{\ell} A_{2\ell+1}^{(2n+1)} \sin[(2\ell+1)\theta],\\
\mathrm{se}_{2n+2}\left(\theta,-\frac{\mathrm{Pe}^2}{4}\right) &= (-1)^n \sum_{\ell=0}^{\infty}(-1)^{\ell} B_{2\ell+2}^{(2n+2)} \sin[(2\ell+2)\theta].
\end{aligned} \tag{A.1}$$

The relationship of these functions with the Peclet number is established via the Fourier series coefficients $A_{\ell}^{(n)}$ and $B_{\ell}^{(n)}$ whose values result from recurrence relations and a normalization criterion. In the present work the normalization proposed by Frenkel [39] is adopted.

The chosen normalization along with the orthogonality property of the angular Mathieu functions leads to

$$\begin{aligned}
&\frac{1}{\pi}\int_{-\pi}^{\pi} \mathrm{ce}_n\left(\theta,-\frac{\mathrm{Pe}^2}{4}\right)\mathrm{se}_m\left(\theta,-\frac{\mathrm{Pe}^2}{4}\right)\mathrm{d}\theta = 0 && \forall n,m \geq 0,\\
&\frac{1}{\pi}\int_{-\pi}^{\pi} \mathrm{ce}_n\left(\theta,-\frac{\mathrm{Pe}^2}{4}\right)\mathrm{ce}_m\left(\theta,-\frac{\mathrm{Pe}^2}{4}\right)\mathrm{d}\theta = \varepsilon_n\delta_{nm} && \forall n,m \geq 0,\\
&\frac{1}{\pi}\int_{-\pi}^{\pi} \mathrm{se}_n\left(\theta,-\frac{\mathrm{Pe}^2}{4}\right)\mathrm{se}_m\left(\theta,-\frac{\mathrm{Pe}^2}{4}\right)\mathrm{d}\theta = \delta_{nm} && \forall n,m > 0,
\end{aligned} \tag{A.2}$$

where $\varepsilon_0 = 2$ and $\varepsilon_n = 1$ for all other values of $n$. Additionally, to streamline the expressions given in Eqs. (22) and (35) for the inner solution in the ground, the dummy angular Mathieu function $\mathrm{se}_0$ is introduced and defined as

$$\mathrm{se}_0\left(\theta,-\frac{\mathrm{Pe}^2}{4}\right) = 0. \tag{A.3}$$

Despite the utility and widespread use of the previous expressions for the angular Mathieu functions, the present work introduces alternative expressions that resemble the structure of complex Fourier series expansions:

$$\mathrm{ce}_n\left(\theta,-\frac{\mathrm{Pe}^2}{4}\right) = \sum_{\ell=-\infty}^{\infty} c_{n\ell}\mathrm{e}^{\imath\ell\theta} \qquad \text{and} \qquad \mathrm{se}_n\left(\theta,-\frac{\mathrm{Pe}^2}{4}\right) = \sum_{\ell=-\infty}^{\infty} s_{n\ell}\mathrm{e}^{\imath\ell\theta}. \tag{A.4}$$

Comparing these expansions with the ones given before allows to relate the complex Fourier series coefficients $c_{n\ell}$ and $s_{n\ell}$ with the real ones:

$$c_{n\ell} = \begin{cases} (-1)^{\frac{n+|\ell|}{2}}\dfrac{\varepsilon_n A_{|\ell|}^{(n)}}{2} & \text{for } n \text{ and } \ell \text{ even or } 0,\\ (-1)^{\frac{n+|\ell|-2}{2}}\dfrac{B_{|\ell|}^{(n)}}{2} & \text{for } n \text{ and } \ell \text{ odd},\\ 0 & \text{otherwise.}\end{cases} \tag{A.5}$$

$$s_{n\ell} = \begin{cases} \dfrac{\ell}{|\ell|}(-1)^{\frac{n+|\ell|}{2}}\dfrac{B_{|\ell|}^{(n)}}{2\imath} & \text{for } n \text{ and } \ell \text{ even } \neq 0,\\ \dfrac{\ell}{|\ell|}(-1)^{\frac{n+|\ell|-2}{2}}\dfrac{A_{|\ell|}^{(n)}}{2\imath} & \text{for } n \text{ and } \ell \text{ odd},\\ 0 & \text{otherwise.}\end{cases} \tag{A.6}$$

### A.1. Limit of creeping groundwater flows

Angular Mathieu functions depend on the Peclet number of the groundwater flow through the real Fourier series coefficients $A_{\ell}^{(n)}$ and $B_{\ell}^{(n)}$, or alternatively, through $c_{n\ell}$ and $s_{n\ell}$. This subsection examines the behavior of the aforementioned coefficients to thereafter present the expansion of angular Mathieu functions in the limit of creeping groundwater flows.

Literature shows that angular Mathieu functions can be expanded into power series of their second parameter, $-\mathrm{Pe}^2/4$ in this case [31,32,39]. Therefore, Fourier series coefficients $A_\ell^{(n)}$ and $B_\ell^{(n)}$ can be written, in first approximation, as

$$A_\ell^{(n)}\Big|_{\mathrm{Pe}\ll 1} = B_\ell^{(n)}\Big|_{\mathrm{Pe}\ll 1} = 1 + \mathcal{O}\left(\mathrm{Pe}^2\right) \qquad \text{if } \ell = n, \text{ or}$$

$$A_\ell^{(n)}\Big|_{\mathrm{Pe}\ll 1} = B_\ell^{(n)}\Big|_{\mathrm{Pe}\ll 1} = \mathcal{O}\left(\mathrm{Pe}^{2|n-\ell|}\right) \qquad \text{if } \ell \neq n. \tag{A.7}$$

These expansions are substituted into Eq. (A.5) and (A.6) to obtain the behavior of $c_{n\ell}$ and $s_{n\ell}$ in the limit of creeping groundwater flows:

$$c_{n\ell}\Big|_{\mathrm{Pe}\ll 1} = \frac{\epsilon_n \delta_{n|\ell|}}{2} + \mathcal{O}\left(\mathrm{Pe}^2\right) \qquad \text{and} \qquad s_{n\ell}\Big|_{\mathrm{Pe}\ll 1} = \frac{\ell}{|\ell|}\frac{\delta_{n|\ell|}}{2\imath}(1-\delta_{|\ell|0}) + \mathcal{O}\left(\mathrm{Pe}^2\right). \tag{A.8}$$

Finally, the first approximation of the angular Mathieu functions in the limit of interest is obtained by substituting the above results for $c_{n\ell}$ and $s_{n\ell}$ into Eq. (A.4), leading to

$$\mathrm{ce}_n\left(\theta, -\frac{\mathrm{Pe}^2}{4}\right)\Big|_{\mathrm{Pe}\ll 1} = \frac{\mathrm{e}^{\imath n\theta} + \mathrm{e}^{-\imath n\theta}}{2} + \mathcal{O}\left(\mathrm{Pe}^2\right) \qquad \text{and} \qquad \mathrm{se}_n\left(\theta, -\frac{\mathrm{Pe}^2}{4}\right)\Big|_{\mathrm{Pe}\ll 1} = \frac{\mathrm{e}^{\imath n\theta} - \mathrm{e}^{-\imath n\theta}}{2\imath} + \mathcal{O}\left(\mathrm{Pe}^2\right). \tag{A.9}$$

It becomes evident that angular Mathieu functions $\mathrm{ce}_n$ and $\mathrm{se}_n$ tend to $\cos(n\theta)$ and $\sin(n\theta)$, respectively, for small values of their second argument, $-\mathrm{Pe}^2/4$ in this case. This behavior is the reason why angular Mathieu functions are also known in the literature as elliptical cosines and sines [52].

## Appendix B. Modified Mathieu functions

Modified Mathieu functions can be expressed in many different ways [32]. For convenience, in the present work these are written as series of cross-products of modified Bessel functions of the first and second kind, $\mathrm{I}_n$ and $\mathrm{K}_n$ respectively [31]:

$$\begin{aligned}
\mathrm{Ke}_{2n}\left(\ln\rho, \frac{\mathrm{Pe}}{2}\right) &= \frac{1}{\epsilon_n}\sum_{\ell=0}^{\infty}\frac{A_{2\ell}^{(2n)}}{A_{2n}^{(2n)}}\left[\mathrm{I}_{\ell-n}\left(\frac{\mathrm{Pe}}{2}\frac{1}{\rho}\right)\mathrm{K}_{\ell+n}\left(\frac{\mathrm{Pe}}{2}\rho\right) + \mathrm{I}_{\ell+n}\left(\frac{\mathrm{Pe}}{2}\frac{1}{\rho}\right)\mathrm{K}_{\ell-n}\left(\frac{\mathrm{Pe}}{2}\rho\right)\right],\\
\mathrm{Ke}_{2n+1}\left(\ln\rho, \frac{\mathrm{Pe}}{2}\right) &= \sum_{\ell=0}^{\infty}\frac{B_{2\ell+1}^{(2n+1)}}{B_{2n+1}^{(2n+1)}}\left[\mathrm{I}_{\ell-n}\left(\frac{\mathrm{Pe}}{2}\frac{1}{\rho}\right)\mathrm{K}_{\ell+n+1}\left(\frac{\mathrm{Pe}}{2}\rho\right) - \mathrm{I}_{\ell+n+1}\left(\frac{\mathrm{Pe}}{2}\frac{1}{\rho}\right)\mathrm{K}_{\ell-n}\left(\frac{\mathrm{Pe}}{2}\rho\right)\right],\\
\mathrm{Ko}_{2n+2}\left(\ln\rho, \frac{\mathrm{Pe}}{2}\right) &= \sum_{\ell=0}^{\infty}\frac{B_{2\ell+2}^{(2n+2)}}{B_{2n+2}^{(2n+2)}}\left[\mathrm{I}_{\ell-n}\left(\frac{\mathrm{Pe}}{2}\frac{1}{\rho}\right)\mathrm{K}_{\ell+n+2}\left(\frac{\mathrm{Pe}}{2}\rho\right) - \mathrm{I}_{\ell+n+2}\left(\frac{\mathrm{Pe}}{2}\frac{1}{\rho}\right)\mathrm{K}_{\ell-n}\left(\frac{\mathrm{Pe}}{2}\rho\right)\right],\\
\mathrm{Ko}_{2n+1}\left(\ln\rho, \frac{\mathrm{Pe}}{2}\right) &= \sum_{\ell=0}^{\infty}\frac{A_{2\ell+1}^{(2n+1)}}{A_{2n+1}^{(2n+1)}}\left[\mathrm{I}_{\ell-n}\left(\frac{\mathrm{Pe}}{2}\frac{1}{\rho}\right)\mathrm{K}_{\ell+n+1}\left(\frac{\mathrm{Pe}}{2}\rho\right) + \mathrm{I}_{\ell+n+1}\left(\frac{\mathrm{Pe}}{2}\frac{1}{\rho}\right)\mathrm{K}_{\ell-n}\left(\frac{\mathrm{Pe}}{2}\rho\right)\right],
\end{aligned} \tag{B.1}$$

where $\epsilon_0 = 2$ and $\epsilon_n = 1$ for all other values of $n$. Additionally, to streamline the expressions given in Eqs. (22) and (35) for the inner solution in the ground, the dummy modified Mathieu function $\mathrm{Ko}_0$ is introduced and defined as

$$\mathrm{Ko}_0\left(\ln\rho, \frac{\mathrm{Pe}}{2}\right) = 0. \tag{B.2}$$

The following two subsections analyze the behavior of the modified Mathieu functions in two distinguished limits. Firstly, in the intermediate region where $\rho \gg 1$, to facilitate the asymptotic matching of inner and outer solutions presented in Section 4.5. Secondly, in the limit of creeping groundwater flows for which $\mathrm{Pe} \ll 1$, to enable the comparison performed in Section 6 between the developed asymptotic model and the state of the art.

### *B.1. Behavior in the intermediate region*

In this work, modified Mathieu functions are expressed as infinite series, with each term comprising two distinct contributions. The present subsection derives simpler asymptotic expansions to facilitate the matching process of inner and outer solutions. To do so, the potential existence of a dominant term within the series is analyzed next.

All contributions in the series involve modified Bessel functions. For the modified Bessel functions of the first kind $\mathrm{I}_n$, their argument $\mathrm{Pe}/(2\rho)$ is small compared to unity in the intermediate region where $\rho \gg 1$. This enables to identify $\mathrm{I}_0$ as the dominant function among the modified Bessel functions of the first kind [31]. In contrast, at distances far from the borehole, the argument $\mathrm{Pe}\rho/2$ of the modified Bessel function of the second kind $\mathrm{K}_n$ is large compared to unity. Given the behavior of these functions for large values of their argument [31], all modified Bessel functions of the second kind are equally relevant in the intermediate region, regardless of their order.

The previous analysis indicates that, in the intermediate region, a dominant term exists in the infinite series given in Eq. (B.1) which corresponds to the contribution that includes the modified Bessel function of the first kind of order zero $\mathrm{I}_0$. However, for the modified Mathieu function $\mathrm{Ke}_0$, both contributions involve $\mathrm{I}_0$, and therefore, both must be retained for the term $n = \ell = 0$. For all remaining modified Mathieu functions, the first contribution of the term $n = \ell$ dominates. Hence, in the intermediate region, modified Mathieu functions can be simplified as follows:

$$\begin{aligned}
\mathrm{Ke}_0\left(\ln\rho, \frac{\mathrm{Pe}}{2}\right)\Big|_{\rho\gg 1} &= \mathrm{K}_0\left(\frac{\mathrm{Pe}}{2}\rho\right) + \mathcal{O}\left(\frac{1}{\rho}\right),\\
\mathrm{Ke}_m\left(\ln\rho, \frac{\mathrm{Pe}}{2}\right)\Big|_{\rho\gg 1} &= \mathrm{K}_m\left(\frac{\mathrm{Pe}}{2}\rho\right) + \mathcal{O}\left(\frac{1}{\rho^m}\right) \qquad \forall m > 0,\\
\mathrm{Ko}_m\left(\ln\rho, \frac{\mathrm{Pe}}{2}\right)\Big|_{\rho\gg 1} &= \mathrm{K}_m\left(\frac{\mathrm{Pe}}{2}\rho\right) + \mathcal{O}\left(\frac{1}{\rho^m}\right) \qquad \forall m > 0.
\end{aligned} \tag{B.3}$$

Finally, to facilitate the matching with the outer solution, these expressions are further simplified by expanding the modified Bessel functions of the second kind for large values of their argument:

$$\begin{aligned}
&\mathrm{Ke}_m\left(\ln\rho,\frac{\mathrm{Pe}}{2}\right)\Big|_{\rho\gg1} = \frac{\sqrt{\pi}}{\sqrt{\rho\,\mathrm{Pe}}}\mathrm{e}^{-\frac{\rho\mathrm{Pe}}{2}}\left[1+\mathcal{O}\left(\frac{1}{\rho}\right)\right] \qquad \forall m\geq 0,\\
&\mathrm{Ko}_m\left(\ln\rho,\frac{\mathrm{Pe}}{2}\right)\Big|_{\rho\gg1} = \frac{\sqrt{\pi}}{\sqrt{\rho\,\mathrm{Pe}}}\mathrm{e}^{-\frac{\rho\mathrm{Pe}}{2}}\left[1+\mathcal{O}\left(\frac{1}{\rho}\right)\right] \qquad \forall m> 0.
\end{aligned} \tag{B.4}$$

### B.2. Limit of creeping groundwater flows

As shown in the present appendix, modified Mathieu functions are given by cumbersome expressions. Therefore, this subsection aims to derive simplified asymptotic expansions to facilitate the comparisons with the state of the art performed in Section 6. Again, these simpler expressions are obtained by identifying the most relevant contribution within the series defining the modified Mathieu functions.

Each contribution to each term of the series involves modified Bessel functions of the first and second kind. Thus, the primary focus lies in examining the arguments of these functions, considering $\mathrm{Pe}\ll 1$, as they govern all expansions shown next. In contrast to the previous subsection, in the limit of small Peclet numbers the argument of both kinds of modified Bessel functions, $\mathrm{Pe}/(2\rho)$ and $\mathrm{Pe}\rho/2$, are small compared to unity.

Bearing this in mind, two comparisons are carried out to identify the most relevant contribution within the series. For simplicity, these comparisons are exclusively made for the modified Mathieu functions $\mathrm{Ke}_{2n}$ as the discussion is analogous for the other modified Mathieu functions $\mathrm{Ke}_{2n+1}$, $\mathrm{Ko}_{2n+1}$, and $\mathrm{Ko}_{2n+2}$.

The first comparison is carried out between the two contributions within each term of the series. For the trivial case of the modified Mathieu function of order zero, $\mathrm{Ke}_0$, both contributions are equal so both must be retained. For the remaining modified Mathieu functions $\mathrm{Ke}_{2n}$ with $n\neq 0$, an order of magnitude estimation of each contribution in each term of the series is accomplished:

$$\mathrm{Ke}_{2n}\left(\ln\rho,\frac{\mathrm{Pe}}{2}\right) = \underbrace{\mathrm{I}_0\left(\frac{\mathrm{Pe}}{2}\frac{1}{\rho}\right)\mathrm{K}_{2n}\left(\frac{\mathrm{Pe}}{2}\rho\right)}_{\sim\left(\frac{1}{\rho\mathrm{Pe}}\right)^{2n}} + \underbrace{\mathrm{I}_{2n}\left(\frac{\mathrm{Pe}}{2}\frac{1}{\rho}\right)\mathrm{K}_0\left(\frac{\mathrm{Pe}}{2}\rho\right)}_{\sim\left(\frac{\mathrm{Pe}}{\rho}\right)^{2n}\ln(\rho\mathrm{Pe})} + \sum_{\substack{\ell=0\\ \ell\neq n}}^{\infty}\frac{A_{2\ell}^{(2n)}}{A_{2n}^{(2n)}}\left[\underbrace{\mathrm{I}_{\ell-n}\left(\frac{\mathrm{Pe}}{2}\frac{1}{\rho}\right)\mathrm{K}_{\ell+n}\left(\frac{\mathrm{Pe}}{2}\rho\right)}_{\sim\left(\frac{\mathrm{Pe}}{\rho}\right)^{|\ell-n|}\left(\frac{1}{\rho\mathrm{Pe}}\right)^{\ell+n}} + \underbrace{\mathrm{I}_{\ell+n}\left(\frac{\mathrm{Pe}}{2}\frac{1}{\rho}\right)\mathrm{K}_{\ell-n}\left(\frac{\mathrm{Pe}}{2}\rho\right)}_{\sim\left(\frac{\mathrm{Pe}}{\rho}\right)^{\ell+n}\left(\frac{1}{\rho\mathrm{Pe}}\right)^{|\ell-n|}}\right]. \tag{B.5}$$

The first row on the right hand side corresponds to the term $\ell=n$ of the series which is analyzed separately due to the logarithmic instead of potential behavior of the modified Bessel function of the second kind of order zero $\mathrm{K}_0$ [31]. Among them, the second contribution is negligible compared to the first one in the limit of small Peclet numbers. For the remaining terms in the series, with $\ell\neq n$, a comparison of the order of magnitudes of the two contributions shows that the first one always dominates over the second one since $\ell$ and $n$ are always positive integers:

$$\frac{\left(\frac{\mathrm{Pe}}{\rho}\right)^{|\ell-n|}\left(\frac{1}{\rho\,\mathrm{Pe}}\right)^{\ell+n}}{\left(\frac{\mathrm{Pe}}{\rho}\right)^{\ell+n}\left(\frac{1}{\rho\,\mathrm{Pe}}\right)^{|\ell-n|}} \sim \frac{\mathrm{Pe}^{2|\ell-n|}}{\mathrm{Pe}^{2(\ell+n)}} \gg 1. \tag{B.6}$$

These outcomes allow to write, in first approximation, the modified Mathieu functions of even order $\mathrm{Ke}_{2n}$ for small Peclet numbers as

$$\begin{aligned}
&\mathrm{Ke}_0\left(\ln\rho,\frac{\mathrm{Pe}}{2}\right)\Big|_{\mathrm{Pe}\ll1} = \sum_{\ell=0}^{\infty}\frac{A_{2\ell}^{(0)}}{A_0^{(0)}}\mathrm{I}_\ell\left(\frac{\mathrm{Pe}}{2}\frac{1}{\rho}\right)\mathrm{K}_\ell\left(\frac{\mathrm{Pe}}{2}\rho\right),\\
&\mathrm{Ke}_{2n}\left(\ln\rho,\frac{\mathrm{Pe}}{2}\right)\Big|_{\mathrm{Pe}\ll1} = \sum_{\ell=0}^{\infty}\varepsilon_\ell\frac{A_{2\ell}^{(2n)}}{A_{2n}^{(2n)}}\mathrm{I}_{\ell-n}\left(\frac{\mathrm{Pe}}{2}\frac{1}{\rho}\right)\mathrm{K}_{\ell+n}\left(\frac{\mathrm{Pe}}{2}\rho\right)+\mathcal{O}\left(\mathrm{Pe}^{2n}\right),
\end{aligned} \tag{B.7}$$

where $\varepsilon_0=2$ and $\varepsilon_\ell=1$ for all other values of $n$.

These expressions can be further simplified as one of the terms of the series always dominates. For convenience, the modified Mathieu functions of non-zero order are discussed first. That is, $\mathrm{Ke}_{2n}$ with $n\neq 0$. Taking into account the behavior of the real Fourier series coefficients $A_\ell^{(n)}$ given in Appendix A.1, the following order of magnitude results for each term of the series:

$$\mathrm{Ke}_{2n}\left(\ln\rho,\frac{\mathrm{Pe}}{2}\right)\Big|_{\mathrm{Pe}\ll1} = \sum_{\ell=0}^{\infty}\underbrace{\varepsilon_\ell\frac{A_{2\ell}^{(2n)}}{A_{2n}^{(2n)}}\mathrm{I}_{\ell-n}\left(\frac{\mathrm{Pe}}{2}\frac{1}{\rho}\right)\mathrm{K}_{\ell+n}\left(\frac{\mathrm{Pe}}{2}\rho\right)}_{\sim\mathrm{Pe}^{2|\ell-n|}\mathrm{Pe}^{|\ell-n|}\mathrm{Pe}^{-|\ell+n|}}, \tag{B.8}$$

This comparison reveals that, for $n\neq 0$, the term corresponding to $\ell=n$ dominates in the series.

Finally, the modified Mathieu function of order zero, $\mathrm{Ke}_0$, is analyzed. Since the modified Bessel function of the second kind of order zero, $\mathrm{K}_0$, behaves differently, the order of magnitude of the term $\ell=0$ of the series is treated apart, revealing that for creeping groundwater flows the dominant terms of the series is the one corresponding to $\ell=0$:

$$\mathrm{Ke}_0\left(\ln\rho,\frac{\mathrm{Pe}}{2}\right)\Big|_{\mathrm{Pe}\ll1} = \underbrace{\mathrm{I}_0\left(\frac{\mathrm{Pe}}{2}\frac{1}{\rho}\right)\mathrm{K}_0\left(\frac{\mathrm{Pe}}{2}\rho\right)}_{\sim\ln(\rho\mathrm{Pe})} + \underbrace{\sum_{\ell=1}^{\infty}\frac{A_{2\ell}^{(0)}}{A_0^{(0)}}\mathrm{I}_\ell\left(\frac{\mathrm{Pe}}{2}\rho\right)\mathrm{K}_\ell\left(\frac{\mathrm{Pe}}{2}\rho\right)}_{\sim\mathrm{Pe}^{2\ell}}. \tag{B.9}$$

An equivalent analysis is carried out for the other modified Mathieu functions $\mathrm{Ke}_{2n+1}$, $\mathrm{Ko}_{2n+1}$, and $\mathrm{Ko}_{2n+2}$. All results can be condensed into the following two expressions:

$$\begin{aligned}
&\mathrm{Ke}_m\left(\ln\rho,\frac{\mathrm{Pe}}{2}\right)\Big|_{\mathrm{Pe}\ll1} = \mathrm{K}_m\left(\frac{\mathrm{Pe}}{2}\rho\right)+\mathcal{O}\left(\mathrm{Pe}^2\right) \qquad \forall m\geq 0,\\
&\mathrm{Ko}_m\left(\ln\rho,\frac{\mathrm{Pe}}{2}\right)\Big|_{\mathrm{Pe}\ll1} = \mathrm{K}_m\left(\frac{\mathrm{Pe}}{2}\rho\right)+\mathcal{O}\left(\mathrm{Pe}^2\right) \qquad \forall m> 0.
\end{aligned} \tag{B.10}$$

The zeroth order solution to the inner region presents ratios of modified Mathieu functions evaluated at different radial positions. Using the obtained approximations for small Peclet numbers, these ratios can be simplified as follows:

$$\begin{aligned}
&\left.\frac{\mathrm{Ke}_0\left(\ln\rho,\frac{\mathrm{Pe}}{2}\right)}{\mathrm{Ke}_0\left(0,\frac{\mathrm{Pe}}{2}\right)}\right|_{\mathrm{Pe}\ll 1} = \frac{\mathrm{K}_0\left(\frac{\mathrm{Pe}}{2}\rho\right)}{\mathrm{K}_0\left(\frac{\mathrm{Pe}}{2}\right)} + \mathcal{O}\left(\mathrm{Pe}^2\right) = 1 + \frac{\ln\rho}{\ln\left(\frac{\mathrm{Pe}}{4}\right)+\gamma} + \mathcal{O}\left(\mathrm{Pe}^2\right), \\
&\left.\frac{\mathrm{Ke}_m\left(\ln\rho,\frac{\mathrm{Pe}}{2}\right)}{\mathrm{Ke}_m\left(0,\frac{\mathrm{Pe}}{2}\right)}\right|_{\mathrm{Pe}\ll 1} = \frac{\mathrm{K}_m\left(\frac{\mathrm{Pe}}{2}\rho\right)}{\mathrm{K}_m\left(\frac{\mathrm{Pe}}{2}\right)} + \mathcal{O}\left(\mathrm{Pe}^2\right) = \frac{1}{\rho^{|m|}} + \mathcal{O}\left(\mathrm{Pe}^2\right) \qquad \forall m > 0, \\
&\left.\frac{\mathrm{Ko}_m\left(\ln\rho,\frac{\mathrm{Pe}}{2}\right)}{\mathrm{Ko}_m\left(0,\frac{\mathrm{Pe}}{2}\right)}\right|_{\mathrm{Pe}\ll 1} = \frac{\mathrm{K}_m\left(\frac{\mathrm{Pe}}{2}\rho\right)}{\mathrm{K}_m\left(\frac{\mathrm{Pe}}{2}\right)} + \mathcal{O}\left(\mathrm{Pe}^2\right) = \frac{1}{\rho^{|m|}} + \mathcal{O}\left(\mathrm{Pe}^2\right) \qquad \forall m > 0.
\end{aligned} \tag{B.11}$$

## Data availability

Data will be made available on request.

## References


[1] European Union, Directive 2018/2001/EU of the European parliament and of the council of 11 december 2018 on the promotion of the use of energy from renewable sources, 2018.
[2] International Energy Agency, Renewables 2021: Analysis and forecast to 2026, 2021.
[3] T. Elshehabi, M. Alfehaid, Sustainable geothermal energy: A review of challenges and opportunities in deep wells and shallow heat pumps for transitioning professionals, Energies 18 (4) (2025) 811, http://dx.doi.org/10.3390/en18040811.
[4] S. Chen, J. Mao, X. Han, Heat transfer analysis of a vertical ground heat exchanger using numerical simulation and multiple regression model, Energy Build. 129 (2016) 81–91, http://dx.doi.org/10.1016/j.enbuild.2016.07.010.
[5] A.D. Chiasson, S.J. Rees, J.D. Spitler, A preliminary assessment of the effects of groundwater flow on closed-loop ground-source heat pump systems, ASHRAE Trans. 106 (1) (2000) 380–393.
[6] P. Conti, D. Testi, W. Grassi, Transient forced convection from an infinite cylindrical heat source in a saturated darcian porous medium, Int. J. Heat Mass Transfer 117 (2018) 154–166, http://dx.doi.org/10.1016/j.ijheatmasstransfer.2017.10.012.
[7] Y. Nam, R. Ooka, S. Hwang, Development of a numerical model to predict heat exchange rates for a ground-source heat pump system, Energy Build. 40 (12) (2008) 2133–2140, http://dx.doi.org/10.1016/j.enbuild.2008.06.004.
[8] Y. Niibori, Y. Iwata, S. Ichinose, G. Fukaya, Design of the BHP system considering the heat transport of groundwater flow, in: Proceedings of the World Geothermal Congress 2005, Antalya, Turkey, 2005.
[9] J. Raymond, R. Therrien, L. Gosselin, R. Lefebvre, Numerical analysis of thermal response tests with a groundwater flow and heat transfer model, Renew. Energy 36 (1) (2011) 315–324, http://dx.doi.org/10.1016/j.renene.2010.06.044.
[10] P. Eskilson, Thermal Analysis of Heat Extraction Boreholes (Ph.D. thesis), Department of Mathematical Physics, Lund Institute of Technology, Lund, Sweden, 1987.
[11] P. Eskilson, J. Claesson, Simulation model for thermally interacting heat extraction boreholes, Numer. Heat Transfer 13 (2) (1988) 149–165, http://dx.doi.org/10.1080/10407788808913609.
[12] G. Hellström, Ground Heat Storage: Thermal Analyses of Duct Storage Systems, I. Theory (Ph.D. thesis), Department of Mathematical Physics, Lund Institute of Technology, Lund, Sweden, 1991.
[13] M. Hermanns, J.M. Rivero, On the quasi-steady limit of the enhanced multipole method for the thermal response of geothermal boreholes, Appl. Therm. Eng. 225 (2023) 120121, http://dx.doi.org/10.1016/j.applthermaleng.2023.120121.
[14] M. Hermanns, J.M. Rivero, On the symmetry properties of the network of thermal resistances representing the thermal response of slender geothermal boreholes, Geothermics 94 (2021) 102078, http://dx.doi.org/10.1016/j.geothermics.2021.102078.
[15] J.M. Rivero, M. Hermanns, Enhanced multipole method for the transient thermal response of slender geothermal boreholes, Int. J. Therm. Sci. 164 (2021) 106531, http://dx.doi.org/10.1016/j.ijthermalsci.2020.106531.
[16] M. Hermanns, J.M. Pérez, Asymptotic analysis of vertical geothermal boreholes in the limit of slowly varying heat injection rates, SIAM J. Appl. Math. 74 (1) (2014) 60–82, http://dx.doi.org/10.1137/130930170.
[17] M. Hermanns, Modelling the thermal response of geothermal heat exchangers using asymptotic expansion techniques, in: Proceedings of the World Geothermal Congress 2020+1, Reykjavik, Iceland, 2021.
[18] J. Rico, M. Hermanns, Thermal interaction of slender geothermal boreholes with creeping groundwater flows, Appl. Therm. Eng. 236 (C) (2024) 121626, http://dx.doi.org/10.1016/j.applthermaleng.2023.121626.
[19] J. Rico, M. Hermanns, On the network of thermal resistances embodying the response of geothermal boreholes to creeping groundwater flows, Int. J. Therm. Sci. 204 (2024) 109222, http://dx.doi.org/10.1016/j.ijthermalsci.2024.109222.
[20] C. Prieto, M. Cimmino, Transient heat transfer in ground heat exchangers under groundwater flow, in: Proceedings of the IGSHPA 2022 Research Conference, Las Vegas, USA, 2022, pp. 182–189, http://dx.doi.org/10.22488/okstate.22.000031.
[21] J. Fadejev, R. Simson, J. Kurnitski, F. Haghighat, A review on energy piles design, sizing and modelling, Energy 122 (2017) 390–407, http://dx.doi.org/10.1016/j.energy.2017.01.097.
[22] D.A. Nield, A. Bejan, Convection in Porous Media, fifth ed., Springer, Cham, 2017.
[23] A. Bejan, Convection Heat Transfer, third ed., Wiley, Hoboken, NJ, 2004.
[24] P. Cheng, Mixed convection about a horizontal cylinder and sphere in a fluid-saturated porous medium, Int. J. Heat Mass Transfer 25 (8) (1982) 1245–1246, http://dx.doi.org/10.1016/0017-9310(82)90219-8.
[25] I. Pop, B. Yan, Forced convection flow past a circular cylinder and a sphere in a darcian fluid at large peclet numbers, Int. Commun. Heat Mass Transfer 25 (2) (1998) 261–267, http://dx.doi.org/10.1016/S0735-1933(98)00013-X.
[26] T. Sano, Unsteady heat transfer from a circular cylinder immersed in a darcy flow, J. Engrg. Math. 14 (3) (1980) 177–190, http://dx.doi.org/10.1007/BF00039314.
[27] N. Diao, Q. Li, Z. Fang, Heat transfer in ground heat exchangers with groundwater advection, Int. J. Therm. Sci. 43 (12) (2004) 1203–1211.
[28] J. Rico, M. Hermanns, Modeling the thermal interaction of geothermal boreholes with aquifers using asymptotic expansion techniques, IOP Conf. Ser.: Earth Environ. Sci. 588 (5) (2020) 052033, http://dx.doi.org/10.1088/1755-1315/588/5/052033.
[29] V. Gnielinski, Turbulent heat transfer in annular spaces – a new comprehensive correlation, Heat Transf. Eng. 36 (9) (2015) 787–789, http://dx.doi.org/10.1080/01457632.2015.962953.
[30] P.A. Lagerstrom, Matched Asymptotic Expansions: Ideas and Techniques, Springer, New York, 1988.
[31] F.W. Olver, D.W. Lozier, R.F. Boisvert, C.W. Clark (Eds.), NIST Handbook of Mathematical Functions, Cambridge University Press, New York, 2010.
[32] N.W. McLachlan, Theory and Application of Mathieu Functions, Publisher To the University Geoffrey Cumberlege, Oxford University Press, 1951.

[33] J. Claesson, G. Hellström, Multipole method to calculate borehole thermal resistances in a borehole heat exchanger, HVAC R Res. 17 (6) (2011) 895–911, http://dx.doi.org/10.1080/10789669.2011.609927.
[34] Comsol Inc, COMSOL Multiphysics Version 5.4. Reference Manual, 2018, https://www.comsol.com/.
[35] M. Hermanns, Fast inverse Laplace transform for the unsteady thermal response of geothermal heat exchangers, AIP Conf. Proc. 2186 (1) (2019) 170002, http://dx.doi.org/10.1063/1.5138081.
[36] D. Amos, Algorithm 644: A portable package for bessel functions of a complex argument and nonnegative order, ACM Trans. Math. Softw. ( TOMS) 12 (3) (1986) 265–273, http://dx.doi.org/10.1145/7921.214331.
[37] J. Claesson, S. Javed, An analytical method to calculate borehole fluid temperatures for time-scales from minutes to decades, ASHRAE Trans. 117 (2) (2011) 279–288.
[38] M. Li, A.C.K. Lai, Review of analytical models for heat transfer by vertical ground heat exchangers (GHEs): A perspective of time and space scales, Appl. Energy 151 (2015) 178–191, http://dx.doi.org/10.1016/j.apenergy.2015.04.070.
[39] D. Frenkel, R. Portugal, Algebraic methods to compute mathieu functions, J. Phys. A: Math. Gen. 34 (17) (2001) 3541, http://dx.doi.org/10.1088/0305-4470/34/17/302.
[40] R. Al-Khoury, N. BniLam, M.M. Arzanfudi, S. Saeid, A spectral model for a moving cylindrical heat source in a conductive-convective domain, Int. J. Heat Mass Transfer 163 (2020) 120517, http://dx.doi.org/10.1016/j.ijheatmasstransfer.2020.120517.
[41] R. Al-Khoury, N. BniLam, M.M. Arzanfudi, S. Saeid, Analytical model for arbitrarily configured neighboring shallow geothermal installations in the presence of groundwater flow, Geothermics 93 (2021) 102063, http://dx.doi.org/10.1016/j.geothermics.2021.102063.
[42] Z. Zhao, Y.-F. Lin, A. Stumpf, X. Wang, Assessing impacts of groundwater on geothermal heat exchangers: A review of methodology and modeling, Renew. Energy 190 (2022) 121–147, http://dx.doi.org/10.1016/j.renene.2022.03.089.
[43] J. Claesson, G. Hellström, Analytical studies of the influence of regional groundwater flow by on the performance of borehole heat exchangers, in: 8th International Conference on Thermal Energy Storage, 2000.
[44] S. Erol, B. François, Multilayer analytical model for vertical ground heat exchanger with groundwater flow, Geothermics 71 (2018) 294–305, http://dx.doi.org/10.1016/j.geothermics.2017.09.008.
[45] J.A. Rivera, P. Blum, P. Bayer, Ground energy balance for borehole heat exchangers: Vertical fluxes, groundwater and storage, Renew. Energy 83 (2015) 1341–1351, http://dx.doi.org/10.1016/j.renene.2015.05.051.
[46] M. Verdoya, C. Pacetti, P. Chiozzi, C. Invernizzi, Thermophysical parameters from laboratory measurements and in-situ tests in borehole heat exchangers, Appl. Therm. Eng. 144 (2018) 711–720, http://dx.doi.org/10.1016/j.applthermaleng.2018.08.039.
[47] Z. Wenke, Z. Linhua, G. Yan, G. Xiang, Z. Hao, Y. Mingzhi, The annual fluctuation of underground temperature response caused by ground heat exchanger in the condition of groundwater seepage, Energy Build. 186 (2019) 37–45, http://dx.doi.org/10.1016/j.enbuild.2019.01.004.
[48] A. Capozza, M.D. Carli, A. Zarrella, Investigations on the influence of aquifers on the ground temperature in ground-source heat pump operation, Appl. Energy 107 (2013) 350–363, http://dx.doi.org/10.1016/j.apenergy.2013.02.043.
[49] T. Metzger, S. Didierjean, D. Maillet, Optimal experimental estimation of thermal dispersion coefficients in porous media, Int. J. Heat Mass Transfer 47 (2004) 3341–3353, http://dx.doi.org/10.1016/j.ijheatmasstransfer.2004.02.024.
[50] A. Kashevarov, Exact solution of the problem of convective heat exchange for a circular cylinder at small prandtl numbers, Fluid Dyn. 29 (1) (1994) 33–37, http://dx.doi.org/10.1007/BF02330618.
[51] S. Tomotika, H. Yosinobu, On the convection of heat from cylinders immersed in a low-speed stream of incompressible fluid, J. Math. Phys. 36 (1–4) (1957) 112–120, http://dx.doi.org/10.1002/sapm1957361112.
[52] J.C. Gutiérrez-Vega, R. Rodríguez-Dagnino, M. Meneses-Nava, S. Chávez-Cerda, Mathieu functions, a visual approach, Am. J. Phys. 71 (3) (2003) 233–242, http://dx.doi.org/10.1119/1.1522698.